FERROMAGNETIC JEFFREY NANOFLUID FLOW INFLUENCED BY MAGNETIC DIPOLE WITH CATTANEO-CHRISTOV DOUBLE DIFFUSION AND GYROTACT MICROORGANISM

Student Name: Iqra Rauf
Enrollment No: 01-248202-005
Supervised by Prof. Dr. M. Ramzan

A thesis submitted in fulfilment of the requirements for the award of degree of Masters of Science (Mathematics)

Department of Computer Science

BAHRIA UNIVERSITY ISLAMABAD

SESSION(2020-2022)

Approval of Examination

Scholar Name: Iqra Rauf
Registration Number: 71097
Enrollment: 01-248202-005
Program of Study: MS (Mathematics)
Thesis Title: Ferromagnetic Jeffrey Nanofluid Flow Influenced By Magnetic Dipole With Cattaneo-Christov Double Diffusion and Gyrotactic Microorganism

It is to certify that the above scholar's thesis has been completed to my satisfaction and, to my belief, its standard is appropriate for submission for examination. I have also conducted plagiarism test of this thesis using HEC prescribed software and found similarity index 12%. that is within the permissible limit set by the HEC for the MS/M.Phil degree thesis. I have also found the thesis in a format recognized by the BU for the MS/M.Phil thesis.

Principal Supervisor Name: Prof. Dr. M. Ramzan

Principal Supervisor Signature: 

Date: 12-10-2022

Author's Declaration

I, Iqra Rauf hereby state that my MS/M.Phil thesis titled is my own work and has not been submitted previously by me for taking any degree from Bahria university or anywhere else in the country/world. At any time if my statement is found to be incorrect even after my graduation, the University has the right to withdraw/cancel my MS/M.Phil degree.

Scholar Name: Iqra Rauf

Date: 12-10-2022

Plagiarism Undertaking

I, solemnly declare that research work presented in the thesis titled "Ferromagnetic Jeffrey Nanofluid Flow Influenced By Magnetic Dipole With Cattaneo-Christov Double Diffusion and Gyrotactic Microorganism" is solely my research work with no significant contribution from any other person. Small contribution / help wherever taken has been duly acknowledged and that complete thesis has been written by me. I understand the zero tolerance policy of the HEC and Bahria University towards plagiarism. Therefore I as an Author of the above titled thesis declare that no portion of my thesis has been plagiarized and any material used as reference is properly referred / cited.

I undertake that if I am found guilty of any formal plagiarism in the above titled thesis even after award of MS/M.Phil degree, the university reserves the right to withdraw / revoke my MS/M.Phil degree and that HEC and the University has the right to publish my name on the HEC / University website on which names of scholars are placed who submitted plagiarized thesis.

Scholar Name: Iqra Rauf

Date: 12-10-2022

Dedicated to my Beloved Parents and Respected Supervisor

Acknowledgements

All praises to Almighty Allah, the creator of all the creatures in the universe, who has created us in the structure of human beings as the best creature. Many thanks to Him, who created us as a muslim and blessed us with knowledge to differentiate between right and wrong. Many many thanks to Him as he blessed us with the Holy Prophet, Hazrat Muhammad (Sallallahu Alaihay Wa'alihi wasalam) for Whom the whole universe is created. He (Sallallahu Alaihay Wa'alihi wasalam) brought us out of darkness and enlightened the way to heaven.

I express my heart-felt gratitude to my supervisor Prof.Dr. M. Ramzan for his passionate interest, superb guidance, and inexhaustible inspiration throughout this investigation. His textural and verbal criticism enable me in formatting this manuscript. My debt of gratitude goes to all my respectable teachers especially Dr.Jafar Hasnain and Dr. Rizwan ul Haq for their inspirational guidance. May Almighty Allah shower His choicest blessings and prosperity on all those who assisted me in any way during completion of my thesis. I would like to express my special thanks to Ms Hina Gul who were always remained helpful to me and my friend Zulfiqar Ali. May Allah shower His blessings upon them more than enough.

Abstract

This thesis discusses the flow of Jeffrey nanofluid flow over a stretched surface influenced by magnetic dipole. The flow is subjected to the gyrotactic microorganism that is used to enhance the stability of the fluid. The customary Fourier law owing to its short comings is replaced by the Cattaneo-Christov heat flux. The convective conditions are taken at the boundary of the surface. The envisioned model is solved numerically using bvp4c, a MATLAB built in function. The graphical illustrations are presented to show the relation between the arising parameters with the associated profiles. The salient outcome reveals that temperature and concentration profiles show rising behavior for thermophoresis parameter.

TABLE OF CONTENTS

LIST OF TABLES

LIST OF FIGURES

LIST OF SYMBOLS

M_a	Melting parameter
Sc	Schmidt number
N_t	Thermophoresis parameter
ε	Curie temperature
N_b	Brownian motion
β	Ferro hydrodynamic interaction parameter
D_c	Heat generation parameter
Pr	Prandtl number
R_c	Reaction rate constant
Ec	Eckert number
E_a	Activation energy parameter
c	Stretching parameter
u, v	Components of velocity along x and y-axis (m/s)
T	Nanofluid temperature
T_w	Nanofluid temperature near the wall (k)
T_c	Nanofluid free stream temperature (k)
k	Thermal conductivity
T_∞	Ambient Temperature
u_w	Stretching Coefficient
M	Magnetic effect
C_p	Specific heat
θ_1, θ_2	Fluid temperature
Φ	Magnetic dipole scalar potential
γ	Deborah number

λ	Viscous dissipation factor
Pe	Peclet number
Le	Lewis number
Σ	Microorganism concentration difference parameter
Lb	Bio-convection Lewis number
δ_c	Concentration relaxation parameter
β_{i1}	Biot number
σ	Microorganism concentration difference parameter
wc	Maximum swimming speed for bacteria
D_n	Diffusivity coefficient for microorganisms
γ^*	Dimensionless thermal relaxation time parameter
λ_1	Relaxation time parameter
λ_2	Retardation time parameter
λ_3	Thermal relaxation time parameter
λ_m	Dimensional concentration relaxation time
∇T	Temperature gradient
D	Mass diffusivity
$C-C$	Cattaneo-Christov
K	Gyromagnetic coefficient
H	Elements of the magnetic

Chapter 1

BASIC PRELIMINARIES

This chapter introduces some fundamental definitions, concepts, and laws that will aid comprehension of the works in the following two chapters.

1.1 Fluid

When shear stress is applied to a material, it can flow and deform continuously. Fluids include mercury, cooking oil, blood, and oxygen.

1.2 Nanofluid

The term "nanofluid" refers to a fluid that contains nanoparticles made of metals, oxides, carbon nanotubes, or both. These fluid nanoparticles are primarily used to improve the fluid's thermal conductivity and heat transfer.

1.3 Fluid mechanics

Fluid mechanics is the branch of science that examines gases and liquids both in motion and at rest. There are two categories of fluid.

1.3.1 Fluid statics

A sub-field of fluid mechanics called fluid statics that examine fluids not moving relative to one another.

1.3.2 Fluid dynamics

A branch of fluid mechanics that studies the behaviour of moving fluid.

1.3.3 Viscosity

The natural property of a fluid called viscosity measures the fluid's resistance to any gradual deformation when various forces are applied to it. It is separated into two types. Numerically, it can be addressed as follows:

$$\text{viscosity } = \frac{\text{Shear stress}}{\text{Gradient of velocity}}. \tag{1.1}$$

1.3.4 Dynamic viscosity (μ)

It is a measurement of fluid flow resistance. It has the dimensions $ML^{-1}T^{-1}$ and the units are Kg/ms.

1.3.5 Kinematic viscosity (ν)

The fluid density (ρ) and the dynamic viscosity (μ) ratio is known as kinematic viscosity. It is expressed in SI unit as m^2/s and its dimension is (L^2/T).Mathematically

$$\nu = \frac{\mu}{\rho}. \tag{1.2}$$

1.4 Thermal conductivity

The letter k stands for the unit of measurement for a material capacity to conduct heat. High k values are good thermal conductors, while low k values are either good thermal insulators or poor thermal conductors.

1.5 Thermal diffusivity

It is the ratio of heat stored per unit volume to the heat carried through a medium. The thermal diffusivity increases as heat move through a medium more quickly. A significant amount of heat is absorbed by the material if the thermal diffusivity value is low, whereas a high value implies that heat is mostly absorbed by the substance. Numerically,

$$\alpha = \frac{k}{\rho C_p}, \tag{1.3}$$

where C_p stands for specific heat capacity, k represents thermal conductivity and ρ represents thickness.

1.6 Newton's law of viscosity

If a fluid subjected to mechanical stress,The relationship between shear stress and shear rate is established by Newton's law of viscosity. It can be represented mathematically as follows:

$$\tau_{yx} \propto \frac{du}{dy}, \tag{1.4}$$

or

$$\tau_{yx} = \mu \left(\frac{du}{dy} \right), \tag{1.5}$$

in which τ_{yx} indicate the shear force applied on the fluid's element and μ indicate the absolute viscosity and $\frac{du}{dy}$ indicates the velocity gradient.

1.6.1 Newtonian fluids

Those fluids which obey the Newton law of viscosity and fluid with a constant viscosity. In these fluids shear force (τ_{yx}) is linearly proportional to the gradient of velocity $\left(\frac{du}{dy}\right)$. Alcohol, water, glycerine and kerosene are some examples of Newtonian fluids.

1.6.2 Non-Newtonian fluids

These are the type of fluids which donot obey the Newton law of viscosity. Here, nonlinear and Shear stress ($\boldsymbol{\tau}_{yx}$) and velocity gradient have a direct relationship. In mathematics, it is represented as:

$$\boldsymbol{\tau}_{yx} \propto \left(\frac{du}{dy}\right)^{n}, \; n \neq 1, \tag{1.6}$$

or

$$\boldsymbol{\tau}_{yx} = \eta \frac{du}{dy}, \; \eta = k\left(\frac{du}{dy}\right)^{n-1}, \tag{1.7}$$

where k the consistency index, η represent apparent viscosity and n the flow behaviour index. For $n = 1$ Eq. (1.6) converts to Newton's law of viscosity. Yougurt, fabric paints and ketchup exhibits the non-Newtonian fluid behavior.

1.6.3 Melting heat

The phase change of a substance from a solid to a liquid is caused by a physical process. This happens when a solid internal energy rises, usually due to the application of heat or pressure, raising the temperature to the melting point of the substance. The ordering of ions or molecules in a solid degrades to a less ordered state at the melting point, and the solid "melts" into a liquid.

1.6.4 Activation energy

It is the energy needed to activate particles or atoms so that they can undergo illustrative transformation or physical transport.

1.6.5 Entropy generation

The measure of a system's instability is called entropy. It assists in identifying strategies for reducing or controlling the irreversibility of the system. It is specifically used in channels to study the nano and micro-scales of heat transfer. Entropy generation minimization is a technique used in fuel cells, gas turbines, chillers, and curved pipelines.

1.6.6 Curie temperature

Curie temperature is the point at which some materials cease to possess their intrinsic permanent magnetism, which may usually be replaced by induced magnetism.

1.6.7 Viscous dissipation factor

The irreversible process by which a fluid work on adjacent layers due to shear stresses is turned into heat is known as viscous dissipation.

1.7 Fourier law

According to the Fourier law, the rate of heat transmission through a material is proportional to the area and the negative temperature gradient, through which the heat flow.

$$\mathbf{q} = -k(\nabla T). \tag{1.8}$$

1.8 Cattaneo-Christov heat flux

Two mathematicians, Cattaneo [13] and Christov [14], adapted Fourier law. It may be expressed mathematically as:

$$\mathbf{q} + \lambda_2 \left[\frac{\partial q}{\partial t} + V.\nabla \mathbf{q} - \mathbf{q}.\nabla V + (\nabla .V)\mathbf{q} \right] = -k\nabla T. \tag{1.9}$$

1.9 Dimensionless Numbers

1.9.1 Prandtl number

It measures the difference between thermal and momentum diffusivity. Mathematically

$$\mathrm{Pr} = \frac{\nu}{\alpha} = \frac{\mu C_p}{k}, \tag{1.10}$$

C_p represents specific heat, and k measures thermal conductivity mathematically. The Prandtl number is employed in heat transfer to manage thickness of momentum and thermal boundary

layer.

1.9.2 Nusselt number

The Nusselt number is the proportion of convective to conductive heat transfer at a fluid boundary. Mathematically

$$Nu_L = \frac{h\Delta T}{k\Delta T/L} = \frac{hl}{k}, \tag{1.11}$$

where h represents convective heat transfer, l represents characteristic length, and k denotes thermal conductivity.

1.9.3 Biot number

The Biot number is defined as the ratio of interior diffusion resistance to outside convection resistance. Mathematically

$$\gamma = \frac{h}{k}\sqrt{\frac{\nu}{a}}, \tag{1.12}$$

where kinematic viscosity is ν, the thermal conductivity is k and convective heat transfer coefficient is h.

1.9.4 Eckert number

Eckert number (Ec) stands for the expression of the relationship between the kinetic energy of flow and enthalpy. When the viscous dissipation term in the energy equation is substantial, It is described mathematically as:

$$Ec = \frac{u^2}{C_p \nabla T}, \tag{1.13}$$

wher u represents the continuum's local flow velocity, C_p is local specific heat,ΔT a wall's temperature being different from the surroundings.

1.9.5 Lewis number

Warren Lewis put forward the idea of the Lewis number in 1939 which shows the relationship between Pandit and the Schmidt number. When heat transfer and mass transfer occur Lewis number becomes crucial.

1.9.6 Deborah number

It is the ratio to relax and characterize the time that it consumes for material to set to applied stresses or deformations and the distinguished time scale of an experiment to explore the reaction of the material.

$$De = \frac{\text{Relaxation time}}{\text{Observation time}}. \tag{1.14}$$

1.9.7 Peclet number

The Peclet number is used in convective heat transfer estimates. It refers to the ratio of thermal energy that is transferred to the liquid to thermal energy that is conducted within the liquid.

$$Pe = \frac{\text{Advective transport rate}}{\text{Diffusion transport rate}}. \tag{1.15}$$

where the maximum swimming speed for bacteria is represented by W_c, b is the chemotaxis constant and the diffusivity coefficient for microorganisms is represented as D_n.

1.9.8 Sherwood number

A dimensionless number utilised in mass transfer procedures is the Sherwood number, also referred to as the Nussselt number. Its name honours Thomas Kilgore Sherwood and denotes the proportion of convective mass movement to diffusive mass movement.

$$Sh = \frac{kL}{D}. \tag{1.16}$$

Here D represents mass diffusivity($m^2.s^{-1}$) , L depicts characteristics length (m), and k represents the thermal conductivity.

1.9.9 Thermophoresis parameter

It is the process that stops the mixture of various particles due to a pressure gradient when the particles move collectively or set apart the mixture of the particles after mixing

Thermophoresis is positive on a cold surface and negative on a hot surface.

$$N_t = \frac{(\rho C)_p D_T (T_w - T_c)}{(\rho C)_f \ \nu T_c}, \tag{1.17}$$

T_w and T_c shows the wall temperature and temperature outside the plate, respectively, D_T show the thermophoretic diffusion coefficient, and ν represent the kinematic viscosity.

1.9.10 Brownian motion parameter

It takes place due to the size of the nanoparticles in a nanofluid. Basically, it is a nanoscale process showing nanofluid's thermal influences.

Mathematically

$$N_b = \frac{\tau D_B (C_w - C_c)}{\nu}, \tag{1.18}$$

where

$$\tau = \frac{(\rho C)_p}{(\rho C)_f}. \tag{1.19}$$

1.9.11 Schmidt number

The Schmidt number Sc is a dimensionaless quantity that measures the momentum to mass diffusivity ratio (viscosity). Heinrich Wihel Schmidt is the one who first presented it (1892-1972).

Mathematically

$$Sc = \frac{\nu}{D_B}, \tag{1.20}$$

where ν is kinematic viscosity and D_B is mass diffusivity.

1.10 Fundamental laws

It is necessary to establish some mathematical relations in order to describe the physical behaviour of a fluid flow. We have three basic principles in fluid mechanics that account for fluid motion. These laws are described in their mathematical form as relationships between mass, momentum, and energy rate of change at a point, and are divided into subsections as follows:

1.10.1 Continuity equation

The movement of the conserved quantity is explained by the continuity equation. The conservation of mass, energy, momentum, electric charge, and other natural quantities makes them suitable for use in a variety of physical process equations of continuity. The mass of a closed system stays constant over time since it can only change in quantity by being added or taken away. It represents the fact that mass has a constant value over time. In mathematical form:

$$\frac{d\rho}{dt} + \rho \nabla . V = 0. \tag{1.21}$$

The fluid density is represented by ρ, V represented the velocity field and the material time derivative is represented by d/dt. The time derivative of the material is defined as

$$\frac{d}{dt} = \frac{\partial}{\partial t} + V.\nabla \tag{1.22}$$

Considering Eq. (1.21); Eq. (1.22) has the following form

$$\frac{\partial \rho}{\partial t} + \nabla . (\rho V) = 0 \tag{1.23}$$

For an incompressible fluid,The form of Eq.(1.23) is

$$\nabla . V = 0. \tag{1.24}$$

1.10.2 Momentum equation

The overall linear momentum of a system is constant, according to the conservation of linear momentum concept.

$$\rho \frac{dV}{dt} = \nabla . \tau^* + \rho F \ , \tag{1.25}$$

where F denotes body force vector and τ^* denotes Cauchy stress tensor.

1.10.3 Energy equation

The fluid energy equation is defined as follows:

$$\rho C_p \frac{dT}{dt} = k \nabla^2 T + T. (\nabla V) + Q \ , \tag{1.26}$$

where T denotes temperature, and Q represents the continuous heat source/sink term.

1.10.4 Concentration equation

The concentration equation is defined as follows:

$$\rho \frac{dC}{dt} + V . \nabla C = \rho D^* \nabla^2 C + \frac{\rho D^* k_T}{\nabla T} \nabla^2 T, \tag{1.27}$$

where C stands for concentration. The mass diffusivity coefficient is D, the thermal diffusion ratio is k_T.

1.11 Jeffrey fluid

The rheological effects of linear viscoelastic fluids are described by the Jeffrey fluid model. The time derivative is replaced by the substantive derivative in this model, making it the most basic. It falls under the classification of fluids of the rate type, which explains the properties of both retardation and relaxation time. The Tensor of the Jeffrey Fluid in mathematical form:

$$S = \frac{\mu}{1+\lambda_1}\left(A_1 + \lambda_2 \frac{dA_1}{dt}\right), \tag{1.28}$$

where A_1 is mathematically denoted by $A_1 = \nabla V + (\nabla V)^t$ in Eq. (1.28) in the component form.

$$S_{xx} = \frac{\mu}{1+\lambda_1}\left[2\lambda_2\left(u\frac{\partial}{\partial x} + v\frac{\partial}{\partial y} + w\frac{\partial}{\partial z}\right)\frac{\partial u}{\partial x} + 2\frac{\partial u}{\partial x}\right], \tag{1.29}$$

$$S_{yy} = \frac{\mu}{1+\lambda_1}\left[2\lambda_2\left(u\frac{\partial}{\partial x} + v\frac{\partial}{\partial y} + w\frac{\partial}{\partial z}\right)\frac{\partial v}{\partial y} + 2\frac{\partial v}{\partial y}\right], \tag{1.30}$$

$$S_{zz} = \frac{\mu}{1+\lambda_2}\left[2\lambda_2\left(u\frac{\partial}{\partial x} + v\frac{\partial}{\partial y} + w\frac{\partial}{\partial z}\right)\frac{\partial w}{\partial z} + 2\frac{\partial w}{\partial z}\right], \tag{1.31}$$

$$S_{xy} = S_{yx} = \frac{\mu}{1+\lambda_2}\left[\lambda_2\left(u\frac{\partial}{\partial x} + v\frac{\partial}{\partial y} + w\frac{\partial}{\partial z}\right)\left(\frac{\partial u}{\partial y} + \frac{\partial v}{\partial x}\right) + \left(\frac{\partial u}{\partial y} + \frac{\partial v}{\partial x}\right)\right], \tag{1.32}$$

$$S_{yz} = S_{zy} = \frac{\mu}{1+\lambda_2}\left[\lambda_2\left(u\frac{\partial}{\partial x} + v\frac{\partial}{\partial y} + w\frac{\partial}{\partial z}\right)\left(\frac{\partial v}{\partial z} + \frac{\partial w}{\partial y}\right) + \left(\frac{\partial v}{\partial z} + \frac{\partial w}{\partial y}\right)\right], \tag{1.33}$$

$$S_{xz} = S_{zx} = \frac{\mu}{1+\lambda_2}\left[\lambda_2\left(u\frac{\partial}{\partial x} + v\frac{\partial}{\partial y} + w\frac{\partial}{\partial z}\right)\left(\frac{\partial u}{\partial z} + \frac{\partial w}{\partial x}\right) + \left(\frac{\partial u}{\partial z} + \frac{\partial w}{\partial x}\right)\right], \tag{1.34}$$

Chapter 2

INTRODUCTION AND LITERATURE REVIEW

A fluid containing nanoparticles is known as a nanofluid. The numerous common nanoparticles used in nanofluids include metals, oxides, and carbon nanotubes. The most common fluids used as base are oil, ethylene glycol, and water. Since base fluids are created by dispersing nanoparticles within them, this fluid differs from other conventional base fluids. Thermal conductivity and heat transmission are improved by inclusion of these particles in base fluids. Nanoliquid is a strong contender for the role of working fluid. These particles have a thermal conductivity higher than the base fluid and a size of 1–100 nm and are utilised to improve thermal characteristics at low concentrations. Nanoliquids have the potential to significantly improve heat transfer rates in a variety of zones that use the Navier-Stokes equation, such as nuclear reactors, heat exchangers, industrial cooling applications, transportation, granular insulation, fiber and micro-electromechanical systems granular insulation, chemical catalytic reactors, and the cardiovascular system blood vessels. The improved thermal features of nanofluid benefit micromanufacturing, pharmaceutical processes, power generation, microelectronics, air conditioning, metallurgical, cancer surgery, air conditioning, chemical industries, and so on. Nano particles are needed as coolants in vehicles because of their small size, which requires less energy to manage road resistance. Due to later developments in automotive aerodynamics, there is a great deal of interest in braking systems with more precise heat dis-

sipation and materials like brake nanofluid. Many researchers have recently expressed interest in building more effective solar collectors.Ramzan et al. [1] explored the MHD second-grade nonliquid flow generated by thermal diffusion flux and Cattaneo-Christov concentration over a bi-directional stretched sheet. According to Das et al. [2], nanofluids are mixtures of a base fluid with metallic nanoparticles. Safwa et al. [3] studied magneto nanofluid flow with the dual stratification phenomenon through an absorbent stretching/shrinking surface. Irfan et al. [4-6] described numerous investigations into MHD nanofluids using various models.

Non-Newtonian liquid flows are used in a wide range of industrial and technical processes, including paper production, petroleum drilling, glass blowing, polymeric liquid and melt expulsion, paints, and so on. Non-Newtonian liquids are materials with no direct or linear relationship between shear stress and velocity gradient. There is always a relation between stress and strain rate in non-newtonian liquids. In comparison to Newtonian liquids, the constitutive equations in non-Newtonian liquids are substantially more challenging, nonlinear, and of higher order. These liquids can easily be divided into three groups.

■ At any location, the rate of shear is only specified by the magnitude of shear stress at that instant, so these liquids are stated as time-independent, inelastic, merely viscous, or generalized Newtonian liquids.

■ Time-dependent liquids are more complex liquids in which the duration of shearing, as well as their kinematic history, influences the connection between shear stress and shear rate.

■ Visco-elastic liquids have the properties of both a perfect fluid and an elastic solid, as well as partial elastic recovery after deformation.

These types of liquids are found in many items we use on a daily basis. Shampoo, toothpaste, silly putty, and whipped cream are some of the items on the list. Mathematicians and technologists are well aware that the physics of non-Newtonian liquids presents a unique difficulty. Nonlinearity can manifest itself in a variety of ways in different domains, such as biological engineering and drilling operations. For such liquids, the Navier-Stokes equation is insufficient, and the characteristics of all fluids are not represented by a single fundamental equation in the literature. Consequently, several non-Newtonian fluid models were put forth. Raju et al. [7] inspected 3D Jeffrey fluid flow with the effect of thermal non-linear emission over an extended surface. Hayat et al. [8] described the MHD flow of Jeffrey fluid by a nonlinear radially stretch-

ing surface. Hayat et al. [9] discussed two, the dimensional flow of Jeffrey fluid with the impact of chemical reaction over the extended surface. Imran et al. [10] described the MHD Jeffrey fluid flow with uniform heat flux and chemical reaction over an infinite vertical plate. Waqas et al. [11] created a buoyant thermally radiating stratified Jeffrey nanofluid, whereas Zeeshan et al. [12] observed heat transfer flow of Jeffrey fluid flowing through an uprightly extended surface using a magnetic dipole.

Fourier's original work was recognized as the most acceptable method, which can be used as a guideline for decades because of its widespread applicability. There was a defect in this model that immediately resulted in a parabolic energy equation, meaning that the original disruption was distinguished instantly in the medium. Cattaneo proposed relaxation time to solve the difficulty known as Fourier's law, the "paradox of heat conduction." As can be seen, this correction results in the hyperbolic energy equation, which allows heat to be conveyed by slow-moving thermal waves. Later, Christov improved Cattaneo's model, naming this model (Cattaneo-Christov) C-C heat flux model. Cattaneo [13] solved this problem by incorporating thermal impedance time, which eliminates "heat conduction inconsistency. The Maxwell-Cattaneo model time subsidiary and the Oldroyd upper-convected derivative were combined to change the technique by Christov [14]. Using the Cattaneo method, Khan et al. [15] analyzed the movement and heat transmission in an upper-convicted Maxwell fluid over an exponentially stretched surface. Ramzan et al. [16] explored the modified Fourier law of intensity growth in an MHD third-grade liquid stream with homogenous and heterogeneous responses and boundary conditions through the convection of a directly expanded surface. Rubab et al. [17] discussed the C-C heat flow of a Maxwell fluid boundary layer over an extended sheet. The uniqueness and structural integrity of solutions for controlling the temperature in the C-C heat flow model was established by Tibullo and Zimpoli [18].

A magnetic dipole consists of two magnetic poles separated by a small distance. The combined activities of a magnetic dipole and fluid have been shown to be effective at confining temperature and momentum boundary layers. The heat dissipation phenomenon of fluids is commonly used as heat transporters. The magnetic dipole gradually diminishes the turbulence effects in the flow field. when the source main portion disappears and has no profile. The closed-loop of electric current or a couple of poles are the two forms whose limits are explained

by the magnetic dipole effect. The magnetic source finally becomes a magnetic dipole field when the gap between it and the magnetic field widens. Zeeshan et al. [19] investigated the impact of a magnetic dipole in a ferromagnetic liquid travelling through an extended sheet. Zeeshan et al.[20] explored the heat transfer and flow of Jeffrey fluid with the impact of a magnetic dipole on a linearly stretching surface. Ali et al. [21] explained the magnetic properties of nano-particles on the heat transfer phenomenon with the effect of the magnetic dipole over an extended sheet. Kumar et al. [22] examined the interaction of the Maxwell liquid flow and thermophoretic particle deposition via a stretched surface. Kumar et al. [23] discovered the radiative nanofluid flow with the effect of a magnetic dipole through an extended sheet. Khan et al. [24] conducted a study on thixotropic nanofluids with mass and heat transfer past a curved extended surface on the effect of a magnetic dipole.

Bioconvection is the most common process in suspensions caused by the upward movement of microorganisms with a density slightly greater than water. Bioconvection occurs when the suspension's upper surface becomes too thick due to microbe multiplication, and the microorganisms collapse. Gravitaxis, gyrotaxis, and oxytaxis are all types of microbes. Support from gyrotactic microorganisms in fluids helps with fluid stability, mass conversion, and micro-scale mixing, especially in small quantities. Bioconvection is used in both natural systems and also in biotechnology. The microorganism particles have been widely cast off in the production of mechanical and commercial products such as ethanol, waste-derived biofuel, and compost. Another use of them is in water treatment facilities. Those bacteria deliver hydrogen gas and biodiesel, a possible viable energy source. Numerous remarkable similarities and contrasts exist between motile bacteria and nanoparticles. Self-moving motile bacteria thicken the base liquid by swimming in a specified direction in the liquid in reaction to changes in gravity, light, or material interest. The upper surface of the suspensions becomes flimsy as a result of the grouping of microorganisms, and microorganisms lay down to cause bio-convection. Nanoparticles do not proliferate on their own. These nanoparticles are transferred by the movement of the base fluid and move consequently with processes including Brownian movement and thermophoresis. The gyrotactic microorganism's accumulation into nanofluid increases its solidity as a suspension. Raju et al. [25] looked at the moving wedge being covered by the radiative flow of Casson fluid that contained gyrotactic microorganisms. The

flow of a nanofluid containing gyrotactic microorganisms down a vertical flat plate was studied by Chamkha et al. [26] in the context of natural bioconvection boundary layer flow. In the presence of a magnetic field, Akbar et al. [27] quantitatively examined the shared effects of bioconvection, Brownian motion, gyrotactic nanoparticles, and thermophoresis of gyrotactic microorganisms on a stretching sheet. Waqas et al. [28] investigated the bioconvection of gyrotactic bacteria and nanoparticles in a modified second-grade nanofluid. References [29–32] contain additional observations about the reported bio-convection.

Chapter 3

IRREVERSIBILITY MINIMIZATION ANALYSIS OF FERROMAGNETIC OLDROYD-B NANOFLUID FLOW UNDER THE INFLUENCE OF A MAGNETIC DIPOLE

3.1 Mathematical formulation

We examine $2D$ Oldroyd B nanofluid flow under the influence of a magnetic dipole over a stretching sheet in the x-direction, the surface's distance from the magnetic dipole is "a". which is placed at the centre of y-axis in Fig 3.1. The magnetic dipole generates the magnetic field in the x-direction to saturate the ferrofluid. However, since the temperature T_w is measured at the surface but T_c is assumed at a distance from the sheet, elements won't become magnetic until they begin to cool down close to the thermal boundary layer that is connected to the surface. Here, the Buongiorno nanofluid model is acquired to demonstrate

the effects of Brownian motion and thermophoresis. In this instance, the interaction between activation energy and heat generation is explored, and the melting heat boundary condition is taken into account at the surface.

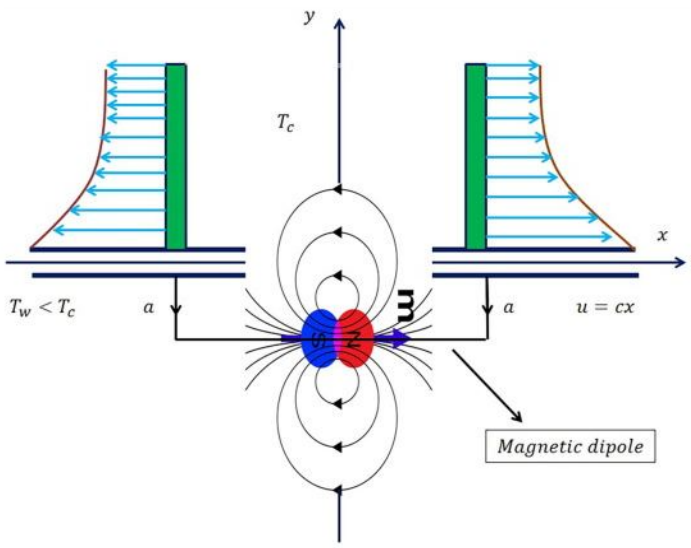

Fig. 3.1 Geometry of the problem [34].

Governing equations

$$\frac{\partial u}{\partial x} + \frac{\partial v}{\partial y} = 0, \tag{3.1}$$

$$v\frac{\partial u}{\partial y} + u\frac{\partial u}{\partial x} + \lambda_1 \left[\begin{array}{c} 2uv\frac{\partial^2 u}{\partial x \partial y} + \\ v^2\frac{\partial^2 u}{\partial y^2} + u^2\frac{\partial^2 u}{\partial x^2} \end{array} \right] = \nu_f \frac{\partial^2 u}{\partial y^2} + \nu_f \lambda_2 \left[\begin{array}{c} v\frac{\partial^3 u}{\partial y^3} - \frac{\partial u}{\partial y}\frac{\partial^2 v}{\partial y^2} + \\ u\frac{\partial^3 u}{\partial x \partial y^2} - \frac{\partial u}{\partial x}\frac{\partial^2 u}{\partial y^2} \end{array} \right] - \frac{\lambda_0 M}{\rho f}\frac{\partial H}{\partial x}, \tag{3.2}$$

$$\begin{aligned} u\frac{\partial T}{\partial x} + v\frac{\partial T}{\partial y} + \lambda_3 \left[\begin{array}{c} u^2\frac{\partial^2 T}{\partial x^2} + v^2\frac{\partial^2 T}{\partial y^2} + 2uv\frac{\partial^2 T}{\partial x \partial y} + \\ v\frac{\partial u}{\partial y}\frac{\partial T}{\partial x} + v\frac{\partial v}{\partial y}\frac{\partial T}{\partial y} + u\frac{\partial v}{\partial x}\frac{\partial T}{\partial y} + u\frac{\partial u}{\partial x}\frac{\partial T}{\partial x} + 2uv\frac{\partial^2 T}{\partial x \partial y} \end{array} \right] \\ = \frac{k_f}{(\rho c_p)_f}\frac{\partial^2 T}{\partial y^2} + \frac{Q_0}{(\rho C_p)_f}(T - T_c) + \tau \left[\begin{array}{c} D_B\frac{\partial C}{\partial y}\frac{\partial T}{\partial y} + \\ \frac{DT}{T_c}\left(\frac{\partial T}{\partial y}\right)^2 \end{array} \right] - \frac{\lambda_0}{(\rho c_p)_f} T\frac{\partial M}{\partial T} \left[\begin{array}{c} u\frac{\partial H}{\partial x} + \\ v\frac{\partial H}{\partial x} \end{array} \right], \end{aligned} \tag{3.3}$$

$$v\frac{\partial C}{\partial y}+u\frac{\partial C}{\partial x}=D_B\left[\frac{\partial^2 C}{\partial y^2}\right]+\frac{D_T}{T_c}\left[\frac{\partial^2 T}{\partial y^2}\right]-k_r^2\left[\frac{T}{T_\infty}\right]^n\exp\left[\frac{-E_a}{kT}\right][C-C_c], \tag{3.4}$$

with the boundary conditions

$$\begin{aligned} v|_{y=0} &= 0,\ u|_{y=0}=u_w=cx,\ \ T|_{y=0}=T_w,\ C|_{y=0}=C_w \\ k\frac{\partial T}{\partial y}|_{y=0} &= \rho_f\left[\lambda^*+c_s(T_w-T)\right]v(x,0) \\ \frac{\partial u}{\partial y}|_{y\to\infty},\ u|_{y\longrightarrow\infty} &\longrightarrow 0,\ T|_{y\longrightarrow\infty}\longrightarrow T_c,\ C|_{y\longrightarrow\infty}\longrightarrow C_c \end{aligned} \tag{3.5}$$

3.1.1 Magnetic dipole appearance

The magnetic dipole scalar possibility Φ is introduced by

$$\Phi=\frac{x\gamma}{2\pi\left(x^2+(\alpha+y)^2\right)}. \tag{3.6}$$

In the above equation , the symbol α stands for the displacement of the magnetic dipole, and the number γ represents the strong point of magnetic field at its base. Magnetic field (H) components are represented mathematically as

$$\frac{\partial H}{\partial x}=-\frac{\partial \Phi}{\partial x}=\frac{\gamma\left[x^2-(\alpha+y)^2\right]}{2\pi\left[x^2+(\alpha+y)^2\right]^2}, \tag{3.7}$$

$$\frac{\partial H}{\partial y}=\frac{-\partial \Phi}{\partial y}=\frac{2x\gamma(\alpha+y)}{2\pi\left[x^2+(\alpha+y)^2\right]^2}, \tag{3.8}$$

$$H=\sqrt{\left(\frac{\partial \Phi}{\partial x}\right)^2+\left(\frac{\partial \Phi}{\partial y}\right)^2}, \tag{3.9}$$

$$\frac{\partial H}{\partial x} = \frac{-2x\gamma}{2\pi(\alpha+y)^4}\ , \tag{3.10}$$

$$\frac{\partial H}{\partial y} = \frac{\gamma}{2\pi}\left[(\frac{-2}{(\alpha+y)^3}+\frac{4x^2}{(\alpha+y)^5})\right], \tag{3.11}$$

The magnetic effect on temperature is given by

$$M = K(T_c - T). \tag{3.12}$$

In this equation, "K" stands for the gyromagnetic coefficient, and for ferromagnetic processes, the applied magnetic field should be non-homogenous and $Tc > T$. When the ferrofluid gains temperature of Tc, There is no need for further magnetization. However, as shown by Eq. (3.12), the fluid is unable to reach the temperature Tc when it is far from the surface.

Similarity transformation are

$$\begin{aligned} u &= cxf^{'}(\eta)\ ,\quad v = \sqrt{-\nu_f c} f(\eta) \quad , \qquad \eta = \sqrt{\frac{c}{\nu_f}} y\ , \quad \xi = \sqrt{\frac{c}{\nu_f}} x, \\ \theta(\xi,\eta) &= \frac{T - T_c}{T_w - T_c} = \theta_1(\eta) + \eta^2 \theta_2(\eta)\ , \quad \phi = \frac{C - C_c}{C_w - C_c} \end{aligned} \tag{3.13}$$

Dimensionless equations are

$$f''' + \beta_2 (f''^2 - f f^{iv}) + f f'' - f'^2 - \beta_1 \left(f^2 f''' - 2 f f' f'' \right) - \frac{2\beta}{(\eta + \alpha)^4} \theta = 0, \tag{3.14}$$

$$\theta_1'' + \Pr \left[\left(\begin{array}{c} f\theta_1' + \phi' \theta_1' N_b \\ + N_t \theta_1'^2 + D_c \theta_1 \end{array} \right) - \gamma^* \left(f^2 \theta_1'' + f f' \theta_1' \right) + \right] + \frac{2\lambda\beta (\theta_1 - \varepsilon) f}{(\eta + \alpha)^3} = 0, \tag{3.15}$$

$$\theta_2'' + \Pr \left[\begin{array}{c} f\theta_2' + \phi' \theta_2' N_b + N_t \theta_2'^2 \\ + D_c \theta_2 - \gamma^* \left(f^2 \theta_2'' + f f' \theta_2' \right) + \end{array} \right] + \frac{2\lambda\beta\theta_2 f}{(\eta + \alpha)^3} - \lambda (\theta_1 - \varepsilon) \beta \left[\begin{array}{c} \frac{2f'}{(\eta+\alpha)^3} \\ + \frac{4f}{(\eta+\alpha)^5} \end{array} \right] = 0, \tag{3.16}$$

$$\phi'' + \frac{N_t}{N_b} \theta'' + Scf\phi' - ScR_c \phi [1 - \alpha_1 \theta]^m \, exp \left[\frac{-E}{1 - \alpha_1 \theta} \right] = 0. \tag{3.17}$$

Boundary conditions of dimensionless equations:

$$\begin{aligned} f'(\eta) &= 1, \Pr f(\eta) + M_a \theta_1'(\eta) = 0, \theta_1(\eta) = 1,\ \theta_2(\eta) = 0, \phi(\eta) = 1, \qquad at\ \eta = 0 \\ f'(\eta) &= 0,\ f''(\eta) = 0, \theta_1(\eta) = 0, \theta_2(\eta) = 0, \phi(\eta) = 0,\ as\ \ \eta \longrightarrow \infty, \end{aligned} \tag{3.18}$$

with

$$\begin{aligned} M_a &= \frac{c_{f(T_c-T_w)}}{\lambda^* + c_s(T_w - T_0)}, \varepsilon = \frac{T_c}{T_c - T_w}, \beta = \frac{\gamma \rho_f \lambda_0 k}{2\pi \mu_0^2}(T_c - T_w), \alpha = a\sqrt{\frac{c\rho_f}{\mu_0}} \\ D_c &= \frac{Q_0}{c(\rho C_p)_f}, Sc = \frac{\nu_f}{D_B}, \gamma^* = \lambda_3 c, E = \frac{-E_a}{kT_c}, E_c = \frac{c^2}{C_p T_0}, \mathrm{Pr} = \frac{\nu_f}{D_B}, R_c = \frac{k_r^2}{c} \\ N_t &= \frac{\tau D_T(T_w - T_c)}{\nu_f}, N_b = \frac{\tau D_B(C_w - C_c)}{\nu_f}, \beta_1 = \lambda_1 c, \beta_2 = \lambda_2 c, \alpha_1 = \frac{k_f}{(\rho C_p)_f}. \end{aligned} \quad (3.19)$$

Sherwood(Sh_x) **and Local Nusselt number**(Nu_x)

Dimensional form of the Nu_x and Sh_x are characterized as:

$$\begin{aligned} Nu_x &= \frac{xq_m}{-k(T_c - T_w)}|_{y=0}\ , Sh_x = \frac{xq_n}{-D_B(C_c - C_w)}|_{y=0}\ , \\ \text{with } q_m &= -k\frac{\partial T}{\partial y}|_{y=0}, \quad q_n = -k\frac{\partial C}{\partial y}|_{y=0} \end{aligned} \quad (3.20)$$

The Nusselt number and the Sherwood number dimensionless forms are:

$$Nu_x Re_x^{-1/2} = [\theta_1^{'}(0) + \xi^2 \theta_2^{'}(0)], ShRe_x^{-1/2} = -\phi^{'}(0). \quad (3.21)$$

where $Re_x = \frac{cx^2}{\nu_f}$ is local Reynolds number.

3.2 Entropy generation

The entropy generation local rate over the stretchings sheet is defined by

$$S_{gen}^{'''} = \frac{K_f}{T_c^2}\left(\frac{\partial T}{\partial y}\right)^2 + \frac{\mu}{T_c}\left[\left(\frac{\partial u}{\partial y}\right)^2 + \lambda_2 \begin{pmatrix} u\frac{\partial u}{\partial y}\frac{\partial^2 u}{\partial x \partial y} \\ +v\frac{\partial^3 u}{\partial y^3} \end{pmatrix}\right] + \frac{RD}{T_c}\left[\frac{\partial C}{\partial y}\right]\left[\frac{\partial T}{\partial y}\right] + \frac{RD}{C_c}\left[\frac{\partial C}{\partial y}\right]^2, \quad (3.22)$$

by similarity transformation the entropy genetration takes the form:

$$
\begin{aligned}
N_G(\eta) &= \frac{S_{gen}''''}{S_0''''} = \frac{S_{gen}''''}{k(\Delta T)^2/L^2T_c^2} \\
&= \alpha_1 \theta'^2 + Re_x Br\left[f''^2 + \beta_2(f'f''^2 - ff''f''')\right] + L\frac{\alpha_2}{\alpha_1}g'^2 + L\theta' g', \qquad (3.23)
\end{aligned}
$$

where

$$
\alpha_1 = \frac{\Delta T}{T_c}, Br = \frac{\mu_f c^2}{C_p k_f T_0}, \alpha_2 = \frac{\Delta C}{Cc}, L = \frac{RD\Delta C}{K_f}. \qquad (3.24)
$$

3.3 Numerical solution

Using the bvp4c MATLAB tool, Eqs (3.14) – (3.17) that correspond to the boundary conditions (3.18) are numerically solved. In order to accomplish this, the higher-order differential equation system under discussion is converted into an order-one system. The tolerance for the given issue is 10^{-5}. The appropriate finite estimate of $\eta \to \infty$ as $\eta_\infty = \eta = 7$ is determined while taking into account the values of the emerging parameter.

$$
\begin{aligned}
f &= y_1,\ f' = y_2,\ \ f'' = y_3,\ \ f''' = y_4, f^{(iv)} = yy_1\ ,\ \theta_1 = y_5, \theta_1' = y_6, \theta_1'' = yy_2, \\
\theta_2 &= y_7,\ \theta_2' = y_8, \theta_2'' = yy_3,\ \phi = y_9,\ \phi' = y_{10}, \phi'' = yy_4, \qquad (3.25)
\end{aligned}
$$

$$
yy_1 = \frac{1}{\beta_2 y_1} = \begin{bmatrix} -y_4 - \beta_2 y_3^2 - y_1 y_3 + y_2^2 + \\ \beta_1\left(y_1^2 y_4 - 2y_1 y_2 y_3 + \frac{2\beta}{(\eta+\alpha)^4} y_5\right) \end{bmatrix}, \qquad (3.26)
$$

$$
yy_2 = \left[\frac{1}{\left(1-\gamma y_1^2\right)}\right]\left[-pr\begin{pmatrix} \left(y_1 y_6 + y_{10} y_6 N_b + N_t y_6^2 + D_c y_5\right) \\ -\gamma^*\left(y_1 y_2 y_6\right) \end{pmatrix} - \frac{2\lambda\beta\left(y_5 - \varepsilon\right)}{\left(\eta+\alpha\right)^3} y_1\right], \qquad (3.27)
$$

$$
yy_3 = \left[\frac{1}{\left(1-\gamma y_2^2\right)}\right]\left[-\Pr\begin{pmatrix} \left(y_1 y_7 + y_{10} y_8 N_b + N_t y_7^2 + D_c y_7\right) \\ -\gamma^*\left(y_1 y_2 y_7\right) - \frac{2\lambda\beta y_7 y_1}{(\eta+\alpha)^3} + \\ \lambda\left(y_5 - \epsilon\right)\beta\left(\frac{2y_2}{(\eta+\alpha)^4} + 4\frac{y_1}{(\eta+\alpha)^5}\right) \end{pmatrix}\right], \qquad (3.28)
$$

$$yy_4 = \frac{-N_t}{N_b} yy_2 - Scy_1 y_{10} + R_c Scy_9 \left(\eta + \alpha\right)^m \exp\left[\frac{-E}{\eta + \alpha_1 y_5}\right], \tag{3.29}$$

The boundary conditions are

$$\begin{aligned} &y_0(2) - 1; \quad \Pr y_0(1) + M_a y_0(6); \quad y_0(7); \; y_0(5) - 1; \; y_0(9) - 1; \\ &y\inf(2); \; y\inf(3); \; y\inf\left(5\right); \; y\inf(7); \; y\inf(9). \end{aligned} \tag{3.30}$$

3.4 Results and discussion

The main goal of this section is to discuss how emerging parameters affect associated distributions in mathematical-modelling. The allowable parameter ranges are as follows

$(0.4 \leq \beta \leq 2.2), (0.1 \leq \beta_1 \leq 1.3), (0.2 \leq \lambda \leq 0.8), (0.1 \leq \gamma^* \leq 0.3),$

$(0.1 \leq D_c \leq 0.4), (0.1 \leq N_b \leq 0.3), (0.0 \leq N_t \leq 0.3), (0.1 \leq R_c \leq 0.4),$

$(0.1 \leq S_c \leq 0.6), (3 \leq \Pr \leq 13), (0.1 \leq M_a \leq 09), (1.0 \leq \alpha_1 \leq 4.0),$

$(0.1 \leq \epsilon \leq 1), (0.1 \leq \alpha \leq 1), (0.1 \leq E_c \leq 3), (0.1 \leq E \leq 1)$

These characteristics are selected on the base of assumptions which provide best graphical result.

Table 3.1: The Sherwood number grid free analysis

$Serial\ No$	Sh_x	$Grid\ size$
1	2.4042	10×10
2	2.4057	50×50
3	2.4058	70×70
4	2.4062	90×90
5	2.4063	100×100
6	2.4064	200×200
7	2.4064	300×300

Table 3.2: Nusselt number for different parameters

$\in$	R_c	N_b	$R_{e_x}^{-\frac{1}{2}} Nu_x$
0.1	0.5		1.79373
0.3			1.64217
0.5			1.47769
0.2	0.1		1.17210
	0.2		1.00430
	0.3		0.88453
	0.5		1.79037
			1.75368
			1.71956
		0.2	1.34590
		0.3	1.16070
		0.4	1.09870

Table 3.3: The Sherwood number for different parameters

Sc	N_b	R_C	$-\phi^{'}(0)$
1.0	0.1	0.1	1.27040
1.5			1.58550
2.0			1.85500
		0.2	1.87980
		0.3	1.90410
		0.4	1.92800
			1.73950
			1.62410
			1.50860
	0.2		1.88660
	0.3		1.91720
	0.4		1.94710

Table 3.4. Comparison of heat transfer rates for impact of prandtl number

Pr	Abel et al. [33]	Chen [34]	Present
0.72	1.0885	1.0885	1.088497
1	1.3333	1.3333	1.333296
3	-	2.5097	2.509689
10	4.7968	4.7968	4.796794

Figure 3.2 display effect of the ferrohydrodynamic interaction parameter β on velocity profile. This clearly indicates that velocity is decreased with an increase in values of β Because of the (ferrohydrodynamic interaction parameter) β, the fluid will become more viscous and have high adhesive forces, and the velocity will appear to be slower. Figures 3.3 and 3.4 show the effect of ferrohydrodynamic interaction parameter β on thermal profiles. There depict the increment in temperature with rising ferrohydrodynamic interaction parameter values. In order to see the impact of the material parameter β_1 on the velocity distribution the outcome is illustrated in

Figure 3.5. The velocity and the boundary layer thickness are both clearly reduced, according to large estimates of β_1. The link between viscous dissipation and temperature distribution is depicted in Figures 3.6 and 3.7. When the effect of viscous dissipation is applied, the thermal of the fluid rises is a well-known fact. Figures 3.8 and 3.9 depict the effect of the thermal relaxation time parameter γ^* on both thermal profiles. It is noticed that the thermal profile and boundary layer thickness are decreased with greater thermal relaxation time parameters. The impact of heat generation parameter D_c on fluid temperature is drawn in Figure 3.10. It is noticed that there is an increase in liquid temperature for D_c. Figure 3.11 and 3.12 are drawn to show how thermophoretic parameters and Brownian motion effect on the concentration profile. Here, opposite trends of the two parameters are evident in relation to the fluid concentration. The concentration profile is decreasing with increased Brownian motion N_b and concentration profile of the fluid increasing with increased value of N_t. The impact of reaction rate constant R_c on the concentration distribution is shown in Figure 3.13. Concentration profile and the thickness of boundary layer boost up through increase in reaction rate constant. Figure 3.14 indicates the effect of melting heat parameter M_a on thermal profile. It shows that the thermal profile is lowered for large values of $M_{a.}$ In Figures $3.15 - 3.17$ the influence of the diffusion variable, Brinkman number, and temperature difference parameter on entropy optimization is shown. The entropy profile is reduced by the temperature difference parameter, but it is increased by the Brinkman number and diffusion variable.

Table 1 Sherwood number grid-free analysis. The numerically calculated Nusselt number for various estimates of the melting heat parameter Curie temperature and dimensionless distance, is shown in Table 2. Evidently, the Nusselt number is falling due to rising estimates for all components. Table 3 shows how the Schmidt number Brownian motion parameter and reaction rate constant all affect the results. It is well known that raising estimates of the Schmidt number, Brownian motion parameter and reaction rate constant increases the concentration rate. Table 4 is constructed to compare the various estimates of the Prandtl number in the limited situation with $Chen$[31] and $Abeletal$[32].

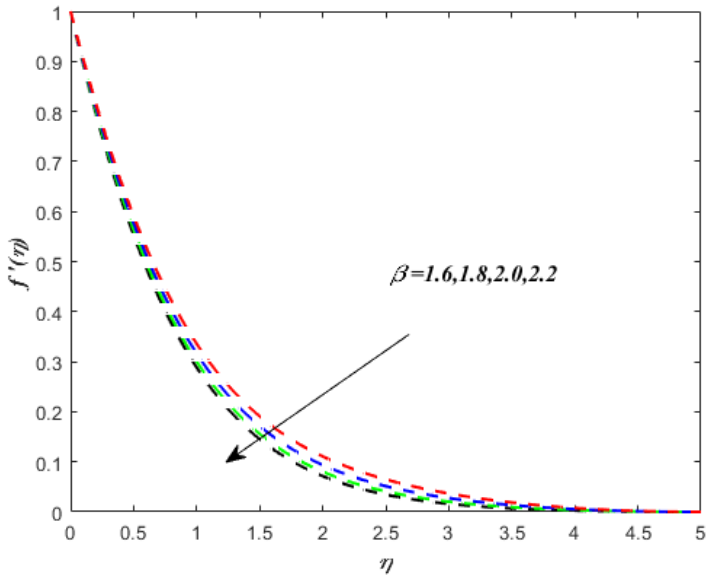

Fig. 3.2 Association of β and $f'(\eta)$.

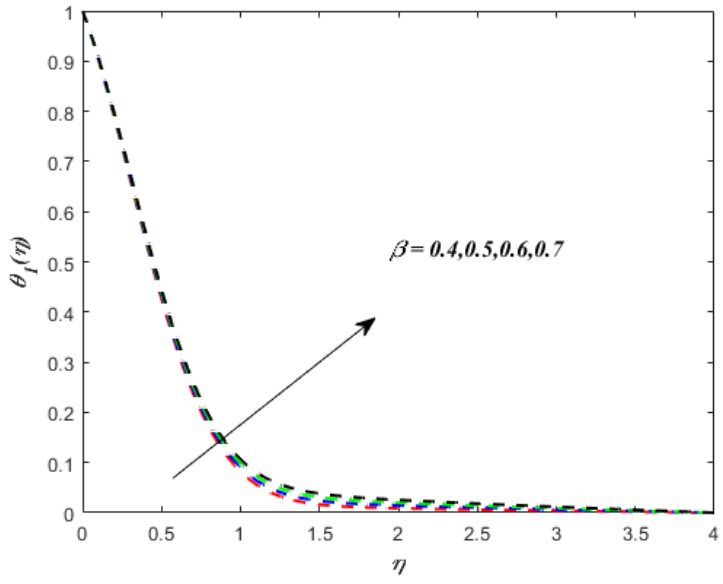

Fig. 3.3 Association of β and $\theta_1(\eta)$.

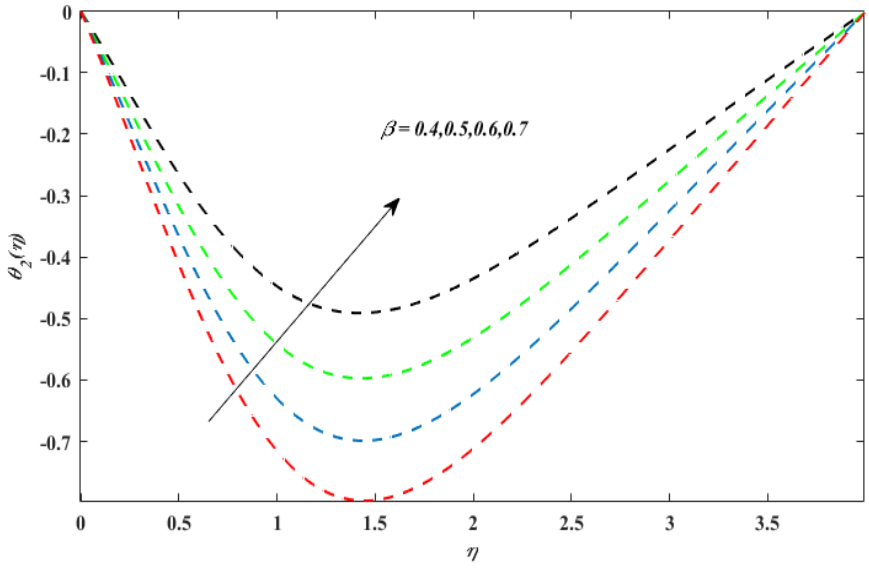

Fig. 3.4 Association of β and $\theta_2(\eta)$.

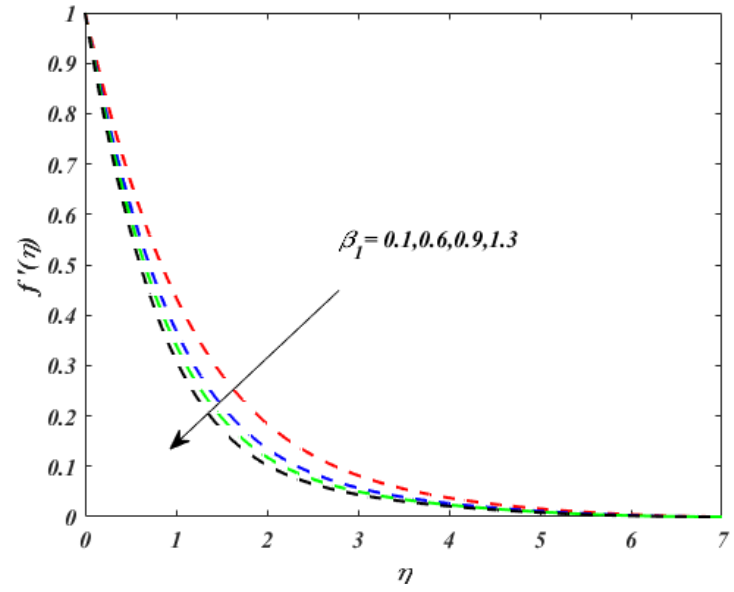

Fig. 3.5 Association of β_1 and $f'(\eta)$.

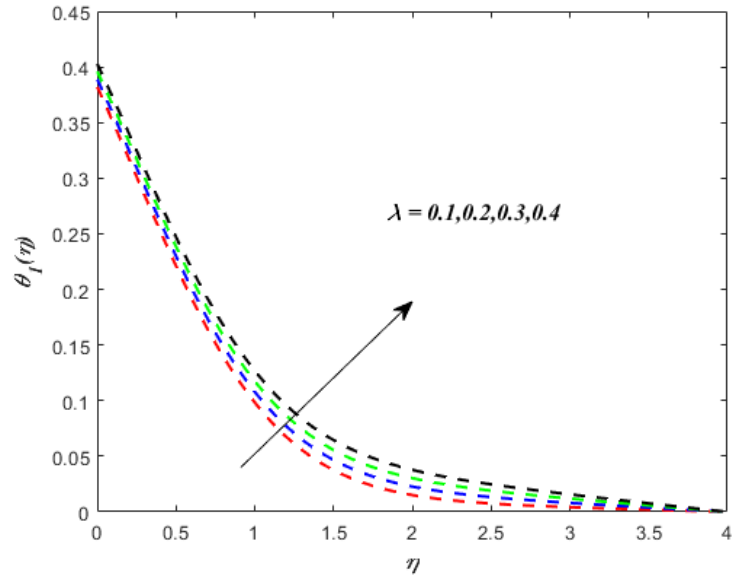

Fig. 3.6 Association of λ and $\theta_1(\eta)$.

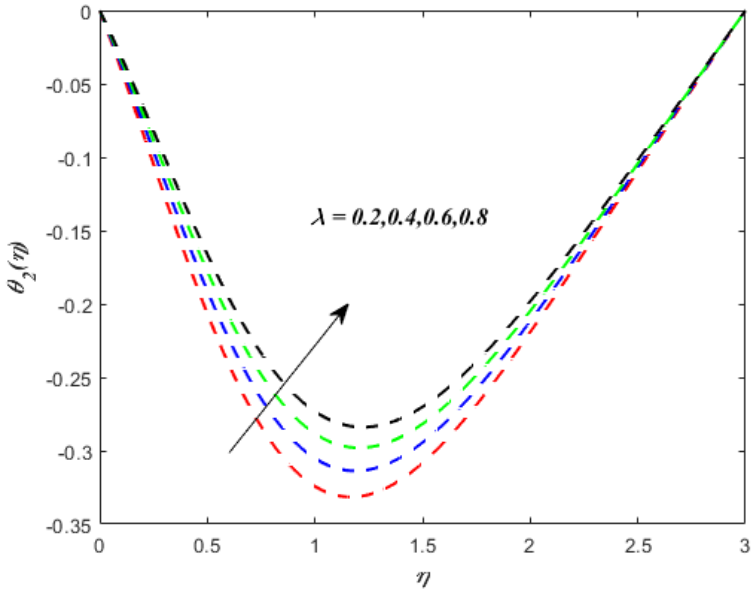

Fig. 3.7 Association of λ and $\theta_2(\eta)$.

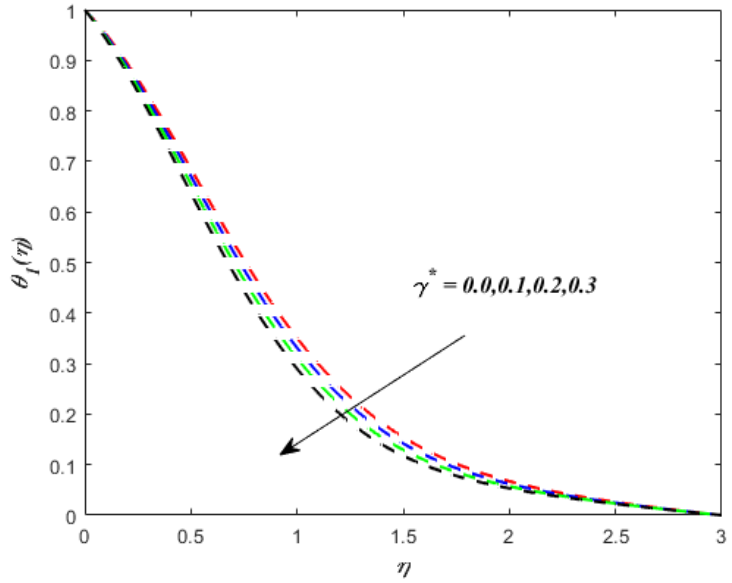

Fig. 3.8 Association of γ^* and $\theta_1(\eta)$.

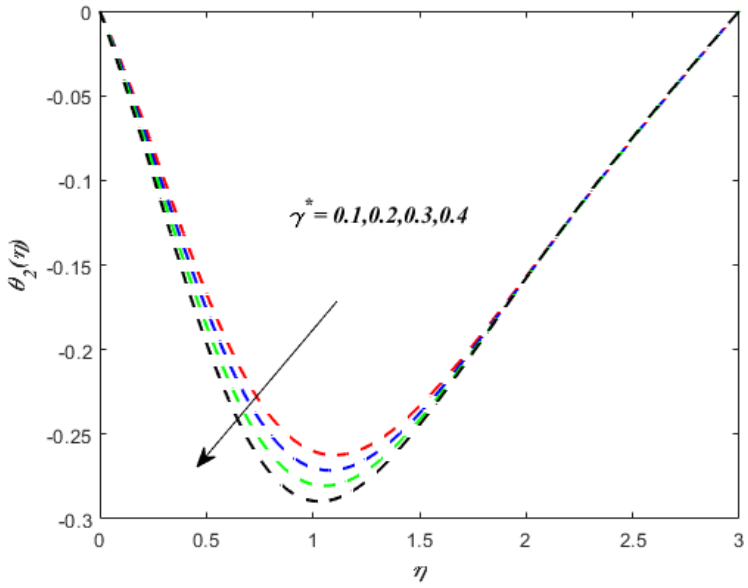

Fig. 3.9 Association of γ^* and $\theta_2(\eta)$.

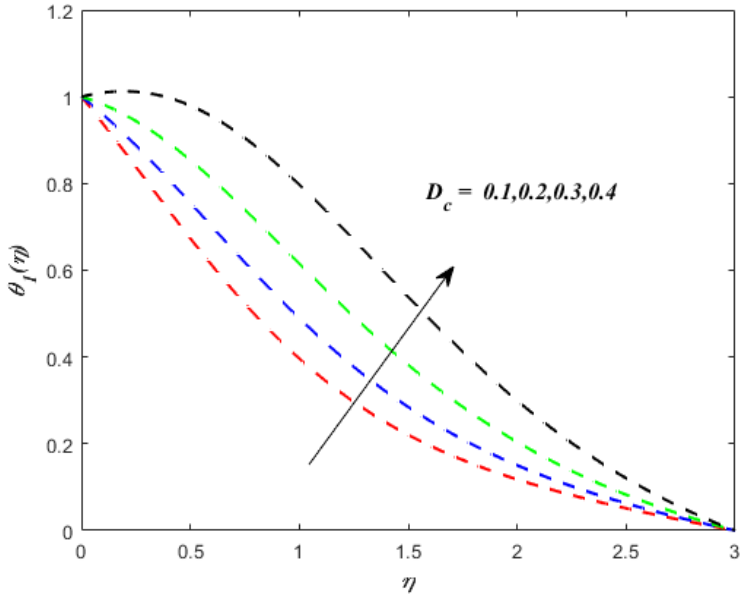

Fig. 3.10 Association of D_c and $\theta_1(\eta)$.

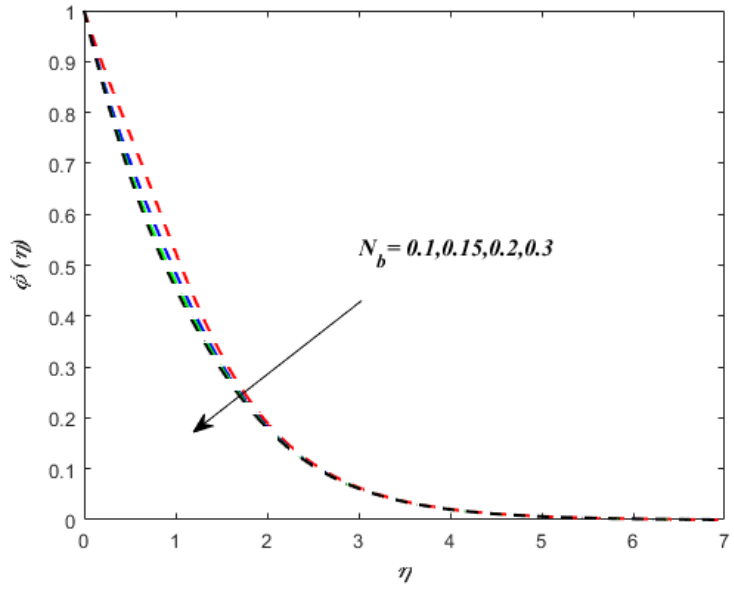

Fig. 3.11 Association of N_b and $\phi(\eta)$.

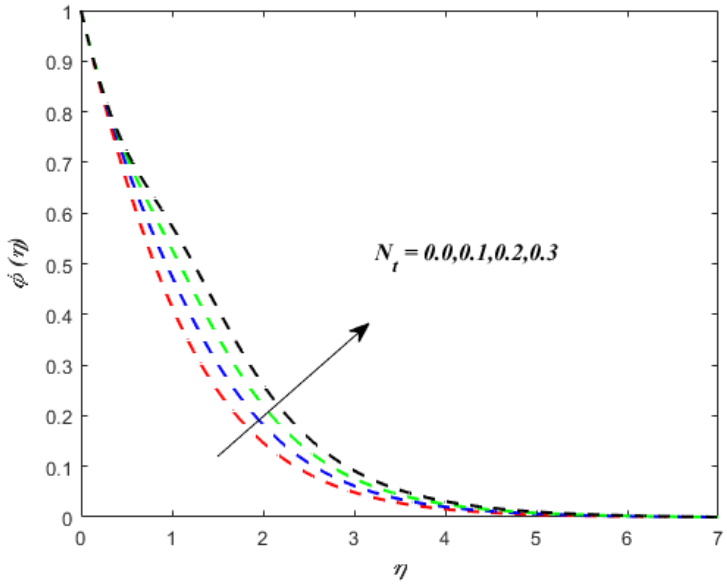

Fig. 3.12 Association of N_t and $\phi(\eta)$.

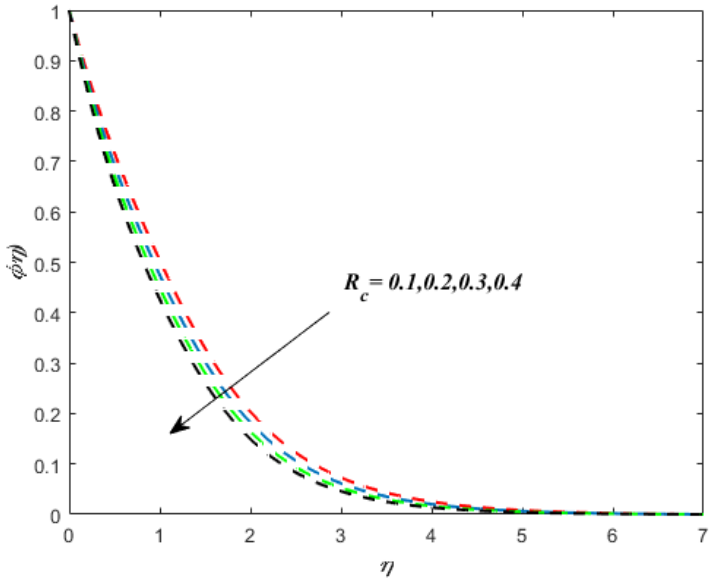

Fig. 3.13 Association of R_c and $\phi(\eta)$.

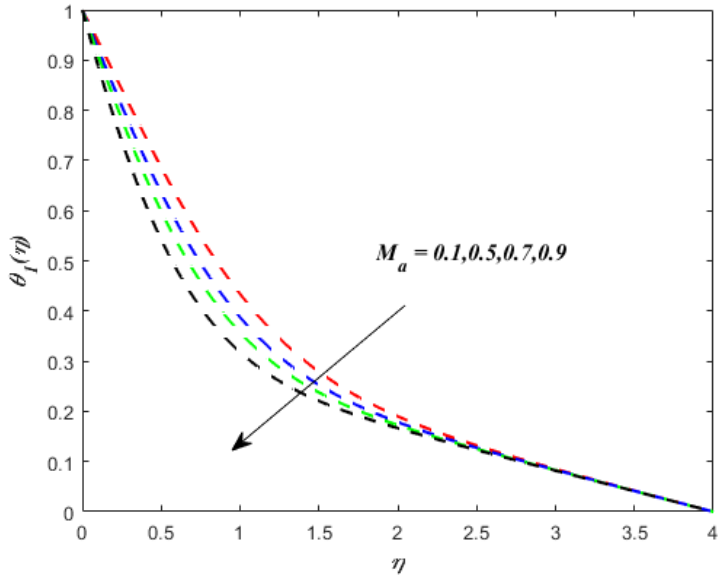

Fig. 3.14 Association of M_a and $\theta_1(\eta)$.

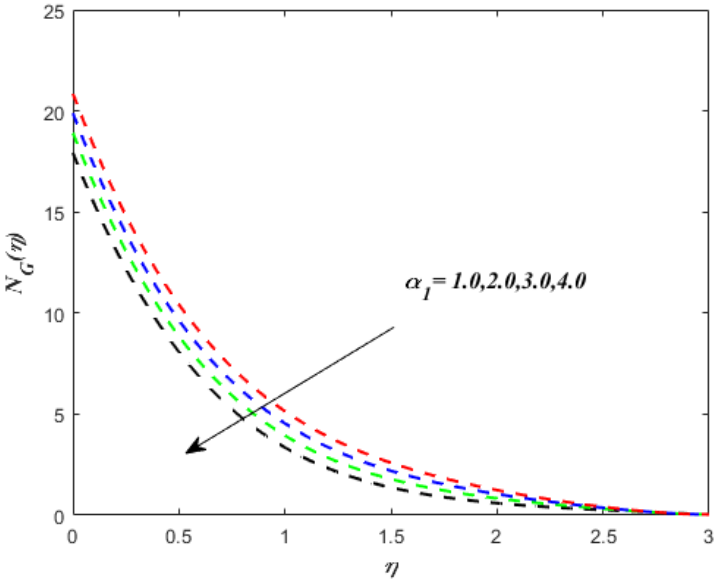

Fig 3.15 Association of α_1 and $N_G(\eta)$.

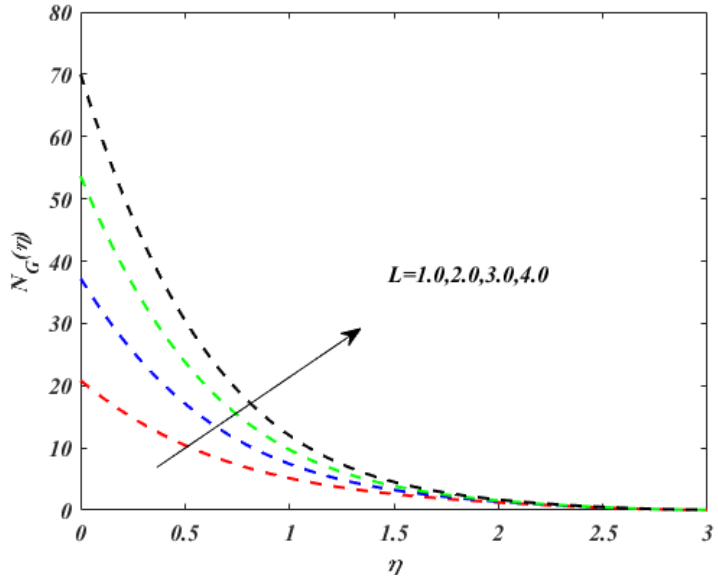

Fig. 3.16 Association of L and $N_G(\eta)$.

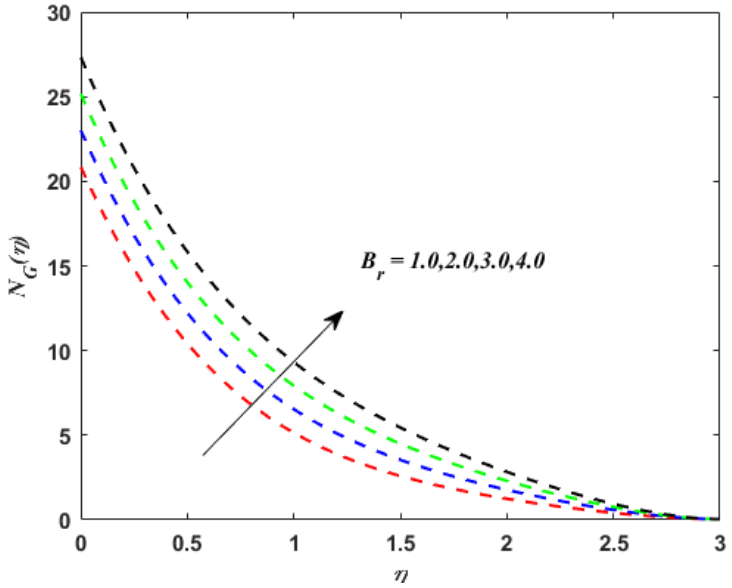

Fig. 3.17 Association of Br and $N_G(\eta)$.

Chapter 4

FERROMAGNETIC JEFFREY NANOFLUID FLOW INFLUENCED BY MAGNETIC DIPOLE WITH CATTANEO CHRISTOV DOUBLE DIFFUSION AND GYROTACTIC MICROORGANISM

In this exploration, two-dimensional incompressible Jeffrey nanofluid flow with bio-convection passing through a stretching surface subjected to a magnetic dipole is studied. The customary Fourier law is replaced by C-C heat flux in this envisioned model. Magnetic nanoparticles play a significant role in the viscoelastic physiognomies of ferrofluid streams. A MATLAB software bvp4c numerical technique is used to address the coupled nonlinear differential equations. Graphs and quantitative data are used to show the impact of various parameters on

velocity, temperature, concentration, and bioconvection profiles. According to the findings, for large values of the thermophoresis parameter, thermal and concentration profiles depict increasing behavior. Moreover, the effects of the viscous dissipation parameter on the temperature field show a rising pattern. The motile density profile declined for greater Lewis and Peclet numbers.

4.1 Problems Development

We study a two-dimensional viscous, incompressible, and electrically non-conducting Jeffery fluid flow that is passing across a stretching surface while subjected to a magnetic field created by a two-pole stretching surface magnet. As shown schematically in Fig 1, an extended surface with velocity $u_w = cx$ is examined along the x-axis, with the y-axis perpendicular to it. The magnetic dipole is positioned at the y-center of the sheet, at a distance of "a" from it. To completely saturate the ferrofluid, the magnetic field strength is increased and orientated in the positive x-direction. The Curie temperature is T_c, while the uniform temperature at the sheet's surface is T_w, and the ambient ferrofluid temperature is T_∞. They won't be able to magnetise until they have cooled.

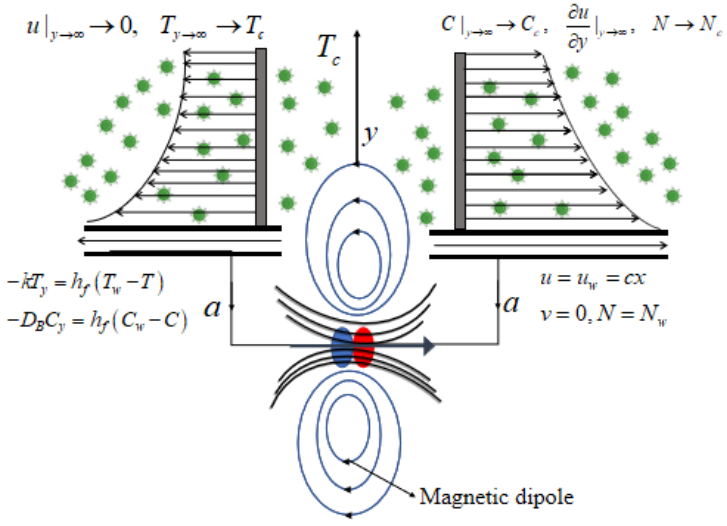

Fig. 4.1 Geometry of the problem.

4.2 Governing equation

Mathematical modeling the governing equations of the assumed system are:

$$\frac{\partial u}{\partial x}+\frac{\partial v}{\partial y}=0, \tag{4.1}$$

$$v\frac{\partial u}{\partial y}+u\frac{\partial u}{\partial x}=\frac{\mu_0}{\rho}M\frac{\partial H}{\partial x}+\frac{v}{1+\lambda_2}\left[\frac{\partial^2 u}{\partial y^2}+\lambda_1\left(u\frac{\partial^3 u}{\partial x\partial y^2}-\frac{\partial u}{\partial x}\frac{\partial^2 u}{\partial y^2}+v\frac{\partial^3 u}{\partial y^3}+\frac{\partial u}{\partial y}\frac{\partial^2 u}{\partial x\partial y}\right)\right], \tag{4.2}$$

$$\begin{aligned} v\frac{\partial T}{\partial y}+u\frac{\partial T}{\partial x}+\lambda_3\left[\begin{array}{c} u^2\frac{\partial^2 T}{\partial x^2}+v^2\frac{\partial^2 T}{\partial y^2}+2uv\frac{\partial^2 T}{\partial x\partial y}+ \\ u\frac{\partial u}{\partial x}\frac{\partial T}{\partial x}+u\frac{\partial v}{\partial x}\frac{\partial T}{\partial y}+v\frac{\partial u}{\partial y}\frac{\partial T}{\partial x}+v\frac{\partial v}{\partial y}\frac{\partial T}{\partial y}\end{array}\right] \\ = \frac{k_f}{(\rho C_p)_f}\frac{\partial^2 T}{\partial y^2}+\tau\left[\begin{array}{c} D_B\frac{\partial C}{\partial y}\frac{\partial T}{\partial y} \\ +\frac{DT}{T_c}\left(\frac{\partial T}{\partial y}\right)^2\end{array}\right]-\frac{\lambda_0}{(\rho C_p)_f}T\frac{\partial M}{\partial T}\left[\begin{array}{c} u\frac{\partial H}{\partial x} \\ +v\frac{\partial H}{\partial x}\end{array}\right], \end{aligned} \tag{4.3}$$

$$v\frac{\partial C}{\partial y}+u\frac{\partial C}{\partial x}+\lambda_m\left[\begin{array}{c} \frac{\partial C}{\partial x}\left(u\frac{\partial u}{\partial x}+v\frac{\partial u}{\partial y}\right)+\frac{\partial C}{\partial y}\left(u\frac{\partial v}{\partial x}+v\frac{\partial v}{\partial y}\right)+ \\ u^2\frac{\partial^2 C}{\partial x^2}+v^2\frac{\partial^2 C}{\partial y2}+2uv\frac{\partial^2 C}{\partial x\partial y}\end{array}\right]=D_B\frac{\partial^2 C}{\partial y^2}+\left[\frac{DT}{T_c}\right]\left[\frac{\partial^2 T}{\partial y^2}\right], \tag{4.4}$$

$$v\frac{\partial N}{\partial y}+u\frac{\partial N}{\partial x}+\frac{bwc}{C_w-C_c}\left[\frac{\partial}{\partial y}\left(N\frac{\partial C}{\partial y}\right)\right]=D_n\frac{\partial^2 N}{\partial y^2}, \tag{4.5}$$

with suitable boundary conditions

$$\begin{aligned} u|_{y=0} &= u_w=cx, v=0, \quad N|_{y=0}=N_w, \\ -kT_y &= h_f\left(T_w-T\right), \quad -D_BC_y=h_f\left(C_w-C\right), \\ u|_{y\to\infty} &\to 0, \quad T|_{y\to\infty}\to T_c, \quad C|_{y\to\infty}\to C_c, \quad N|_{y\to\infty}\to N_c, \quad \frac{\partial u}{\partial y}|_y\to\infty. \end{aligned} \tag{4.6}$$

4.2.1 Magnetic dipole

The permanent magnetic scalar potential of a dipole field is taken as

$$\Phi = \frac{\gamma x}{2\pi\left[x^2 + (\alpha + y)^2\right]}, \tag{4.7}$$

where,the magnetic field's intensity is represented by the symbol γ.

The components of the intensity of the magnetic field along the x and y axes are H_X and H_y, respectively are given as:

$$H_x = -\frac{\partial \Phi}{\partial x} = \frac{\gamma\left[x^2 - (\alpha + y)^2\right]}{2\pi\left[x^2 + (\alpha + y)^2\right]^2}, \tag{4.8}$$

$$H_y = \frac{-\partial \Phi}{\partial y} = \frac{2\gamma x\left[\alpha + y\right]}{2\pi\left[x^2 + (\alpha + y)^2\right]^2}, \tag{4.9}$$

$$H = \left[\left(\frac{\partial \Phi}{\partial x}\right)^2 + \left(\frac{\partial \Phi}{\partial yy}\right)^2\right]^{1/2}, \tag{4.10}$$

$$H_x = \frac{-2x\gamma}{2\pi(\alpha + y)^4}, \tag{4.11}$$

$$H_y = \frac{\gamma}{2\pi}\left[\frac{-2}{(\alpha + y)^3} + \frac{4x^2}{(\alpha + y)^5}\right], \tag{4.12}$$

Magnetization M is a temperature-dependent variables

$$M = K(T_c - T). \tag{4.13}$$

Since K is the gyro-magnetic coefficient in the above calculation, where M is utilized here to represent magnetization.

Similarity Transformations are defined as:

$$\begin{aligned} u &= cxf^{'}(\eta), \quad v = \sqrt{-\nu_f c} f(\eta) \ , \ \eta = \sqrt{\frac{c}{\nu_f}}\, y \ \ , \ \xi = \sqrt{\frac{c}{\nu_f}} x, \\ \theta(\xi, \eta) &= \frac{T - T_c}{T_w - T_c} = \theta_1(\eta) + \eta^2 \theta_2(\eta) \ \ , \ \phi = \frac{C - C_c}{C_w - C_c}, \ \chi = \frac{N - N_c}{N_w - N_c}. \end{aligned} \tag{4.14}$$

Dimensionless equations are as follows:

$$f''' + \gamma\left(f''^{2} - ff^{iv}\right) - (1+\lambda_2)\left(f'^{2} - ff''\right) - (1+\lambda_2)\frac{(2\beta)}{(\eta+\alpha)^4}\theta_1 = 0, \tag{4.15}$$

$$\theta_1'' + \Pr\left[\begin{array}{c} f\theta_1' + \phi'\theta_1' N_b + \\ N_t\theta_1'^2 + D_c\theta_1 \end{array}\right] - \gamma^*\left(f^2\theta_1'' + ff'\theta_1'\right) + \frac{2\lambda\beta\left(\theta_1-\varepsilon\right)f}{(\eta+\alpha)^3} = 0, \tag{4.16}$$

$$\theta_2'' + \Pr\left[\begin{array}{c} f\theta_2' + \phi'\theta_2' N_b + \\ N_t\theta_2'^2 + D_c\theta_2 - \gamma^*\left(f^2\theta_2'' + ff'\theta_2'\right) \end{array}\right] + \frac{2\lambda\beta\theta_2 f}{(\eta+\alpha)^3} - \lambda\left(\theta_1-\varepsilon\right)\beta\left[\begin{array}{c} \frac{2f'}{(\eta+\alpha)^3} + \\ \frac{4f}{(\eta+\alpha)^5} \end{array}\right] = 0, \tag{4.17}$$

$$\phi'' + \theta''\frac{N_t}{N_b} + f\phi' Le - \delta_c Le\left[\begin{array}{c} ff'\phi' \\ +f^2\phi'' \end{array}\right] = 0, \tag{4.18}$$

$$\chi'' + Lbf\chi' - Pe\left[\phi'\chi' + \phi''\left(\chi+\sigma\right)\right] = 0. \tag{4.19}$$

Boundary conditions for dimensionless equations:

$$\begin{aligned} f(0) &= 0,\ f'(0) = 1,\quad \chi(0) = 1,\ \theta_2(0) = 0,\ \theta_1' = -Bi_1\left(1-\theta\right),\quad \phi' = -Bi_2\left(1-\phi\right), \\ f'(\infty) &\to 0,\ f''(\infty) \to 0,\quad \theta_1(\infty) \to 0,\ \theta_2(\infty) \to 0,\ \phi(\infty) \to 0,\ \chi(\infty) \to 0. \end{aligned} \tag{4.20}$$

The above mentioned parameters are translated as:

$$\begin{aligned} \lambda_1 c &= \gamma,\quad Le = \frac{\nu}{D_B},\quad a\lambda_m = \delta_c,\quad L_b = \frac{\nu}{D_n},\quad \sigma = \frac{N_w}{N_w - N_c}, \alpha = a\sqrt{\frac{c\rho_f}{\mu_0}}, \\ \epsilon &= \frac{T_c}{T_c - T_w}, pr = \frac{\nu_f}{\alpha_f},\ Sc = \frac{\nu}{D_B},\ \beta = \frac{\gamma\rho_f\lambda_0 k}{2\pi\mu_0^2}\left(T_c - T_w\right), Pe = \frac{bw_c}{D_n}, \gamma^* = \lambda_3 c, \\ N_t &= \frac{\tau D_T(T_w - T_c)}{T_c\nu_f}, N_b = \frac{\tau D_B(C_w - C_c)}{\nu_f}. \end{aligned} \tag{4.21}$$

4.3 Numerical solutions

Using the bvp4c MATLAB tool, Eqs (4.15) – (4.19) that correspond to the boundary conditions (4.20) are numerically solved. In order to accomplish this, the higher-order differential equation system under discussion is converted into an order-one system. The tolerance for the given issue is 10^{-6}. The appropriate finite estimate of $\eta \to \infty$ as $\eta_\infty = \eta = 9$ is determined while taking into account the values of the emerging parameters.

Below is the algorithim of the numerical Scheme

$$\begin{aligned} f &= y_1,\ f^{'} = y_2,\ f^{''} = y_3,\ f^{'''} = y_4,\ f^{iv} = yy_1\ , \theta_1 = y_5,\ \theta_1^{'} = y_6,\ \theta_1^{''} = yy_2 \\ \theta_2 &= y_7,\ \theta_2^{'} = y_8,\ \theta_2^{''} = yy_3,\ \phi = y_9,\ \phi^{'} = y_{10},\ \phi^{''} = yy_4,\ \chi = y_{11},\ \chi^{'} = y_{12},\ \chi^{''} = yy_5 \end{aligned}$$

Using above Eqs.(4.15) – (4.19) , take the form

$$yy_1 = \frac{1}{\gamma y_1}\left[y_4 + \gamma y_3^2 - (1+\lambda_2)\left(y_2^2 - y_1 y_3\right) - (1+\lambda_2)\frac{(2\beta)}{(\eta+\alpha)^4} y_5\right], \tag{4.22}$$

$$yy_2 = \left(\frac{1}{1-\gamma y_1^2}\right)\left[-pr\begin{pmatrix}(y_1 y_6) + \\ y_9 y_6 N_b + N_t y_6^2\end{pmatrix} - \gamma\left(y_1 y_2 y_6\right)) - \frac{2\lambda\beta\left(y_5 - \varepsilon\right) y_1 y_5}{(\eta+\alpha)^3}\right], \tag{4.23}$$

$$yy_3 = \left(\frac{1}{1-\gamma y_1^2}\right)\begin{bmatrix} -pr\begin{pmatrix}\left(y_1 y_8 + y_{10} y_8 N_b + N_t y_8^2\right)\\ -\gamma\left(y_1 y_2 y_8\right)\end{pmatrix} \\ -\frac{2\lambda\beta y_7 y_1}{(\eta+\alpha)^3} + \lambda\left(y_5 - \varepsilon\right)\beta\left(\frac{2y_2}{(\eta+\alpha)^4} + 4\frac{y_1}{(\eta+\alpha)^5}\right)\end{bmatrix}, \tag{4.24}$$

$$yy_4 = \frac{1}{1-\delta_c Le y_1^2}\begin{bmatrix}\frac{-N_t}{N_b} yy_2 - \delta_c Le y_1 y_{10} \\ +\delta_c Le y_1 y_2 y_{10}\end{bmatrix}, \tag{4.25}$$

$$yy_5 = -Lb y_1 y_{12} + pe\begin{bmatrix} y_{10} y_{12} + \\ yy_4\left(y_{11} + \sigma\right)\end{bmatrix}, \tag{4.26}$$

with the transformed B.CS

$$y_0(2)-1;\ y_0(10)+Bi_2(1-y_0(9));\ y_0(1);y_0(6)+Bi_1(1-y_0(5));\quad y_0(7)$$
$$y_0(11)-1;\quad y\inf(11);\ y\inf(2);y\inf(3);y\inf(5);y\inf(9);y\inf(7) \tag{4.27}$$

4.4 Results and discussion

The main aim of this part has to investigate the outcomes of various appropriate factors including ferrohydrodynamic interaction parameter β, Prandtl no Pr, Deborah number γ, retardation times parameter λ_2, Brownian movement variable N_b, Thermophoresis variable N_t, Dimensionless thermal relaxation time γ^*, Viscous dissipation factor λ, Peclet number Pe, Concentration Lewis number Le, microorganism concentration difference parameter σ, Bio-convection Lewis number Lb and Concentration relaxation parameter δ_c verses the associated profiles.

Figure 4.2 shows the effect of ferrohydrodynamic interaction parameter (β) on the velocity profile. It shows that velocity diminishes as β increments Because of the ferrohydrodynamic interaction parameter, the fluid will become more viscous and have high adhesion forces, and the velocity will appear to be slower. Figure 4.3 depicts the effect of Deborah number (γ) on velocity distribution. It is noted that the Deborah number has an increasing relationship with both boundary layer thickness and velocity. Figure 4.4 shows the impact of the retardation time parameter (λ_2) on the velocity distribution. It is seen that the velocity declines with expanding λ_2 and, consequently, diminishing the boundary layer thickness. Figures 4.5 and 4.6 display the impact of the ferrohydrodynamic interaction parameter (β) on the thermal profile. Here, temperature increments with a higher estimation of β. Figures 4.7 and 4.8 enhance the effect of the dimensionless thermal relaxation time (γ^*) on both thermal profiles. Because of the longer thermal time, the temperature of the liquid drops. Figures 4.9 and 4.10 show the impact of viscous dissipation factor (λ) on temperature distribution. The temperature rises as viscous dissipation increases, as shown by the graphs. Figure 4.11 depicts the influence of the thermophoresis parameter (N_t). As the value of N_t rises, the temperature profile of the fluid rises as well. The reason behind this, the particles of the fluid push the hot fluid away from

the hot surface. Figure 4.12 depicts the relationship between the thermal profile and Prandtl Number (Pr). As (Pr) rises, the relationship becomes more negative.

When the Lewis number (Le) is increased, the boundary layer thickness and nanoparticle concentration decline, as shown in Figure 4.13. For various values of the thermophoresis parameter (N_t) in Figure 4.14,which shows the fluctuations in nanoparticle concentration. In the absence of the N_t, particle concentration is relatively modest. The presence of the Nt increases nanoparticles concentration and the thickness of the boundary layer that surrounds them. The concentration boundary layer shrinks as the concentration relaxation parameter (δ_c) increases, as shown in Figure 4.15. It also indicates that decreasing the value of δ_c improves the concentration movement on the sheet. Figure 4.16 shows the impact of Biot number β_{i1} on concentration profile. It shows the concentration field and boundary layer thickness are increasing at higher Biot numbers. Figures $4.17 - 4.19$ show the impact of Lewis number Lb on motile density profile, bio-convection peclet number Pe, and microorganism concentration difference parameter σ respectively. It is seen that the density profile is decreasing for greater estimates of these parameters.

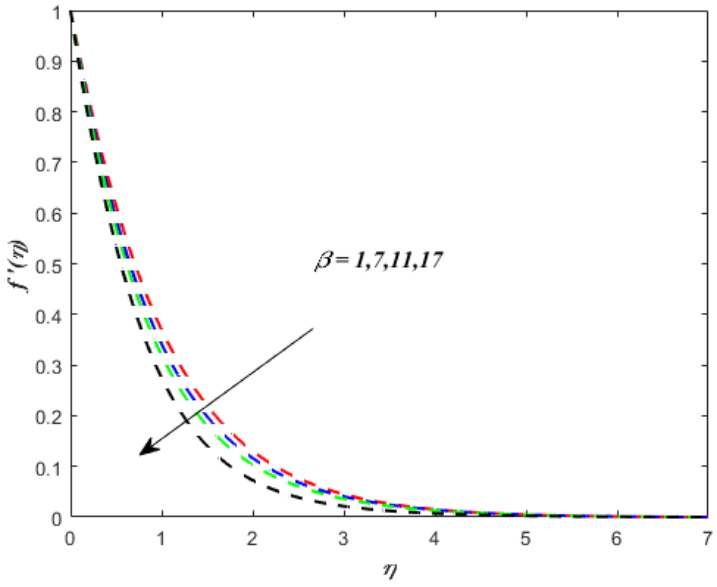

Fig. 4.2. Graph representing effect of $f^{'}$ for several values of β.

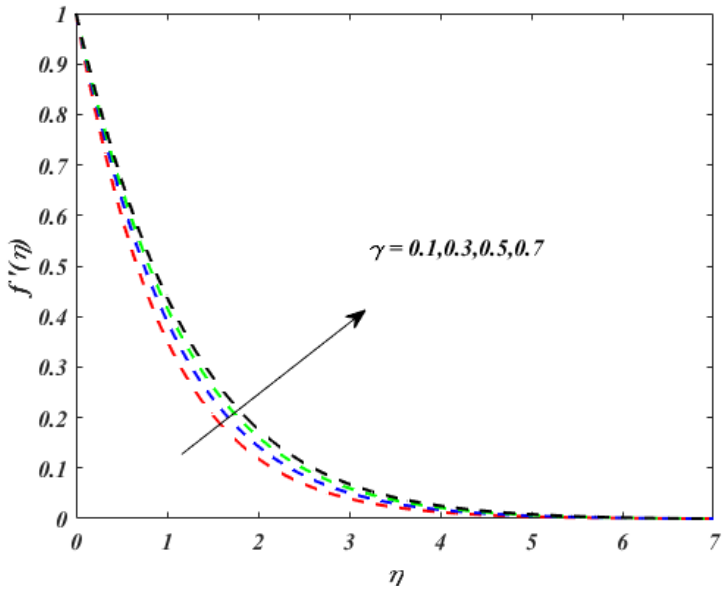

Fig. 4.3. Graph representing effect of f' for several values of γ.

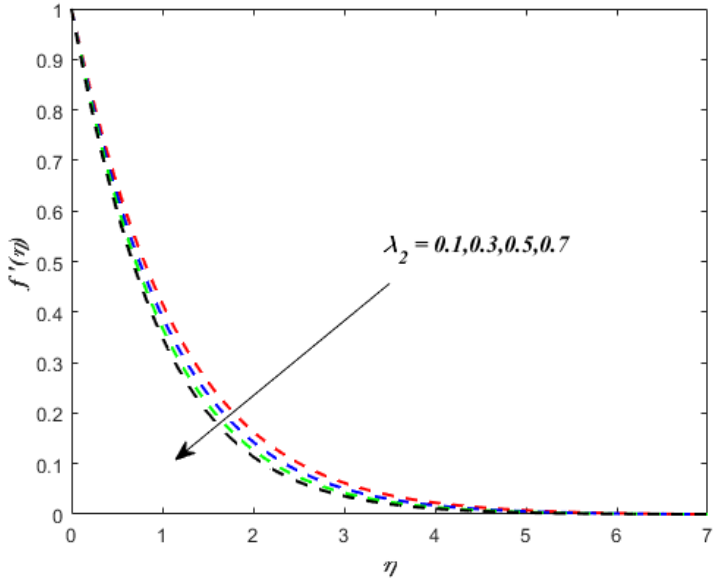

Fig. 4.4. Graph representing effect of f' for several values of λ_2.

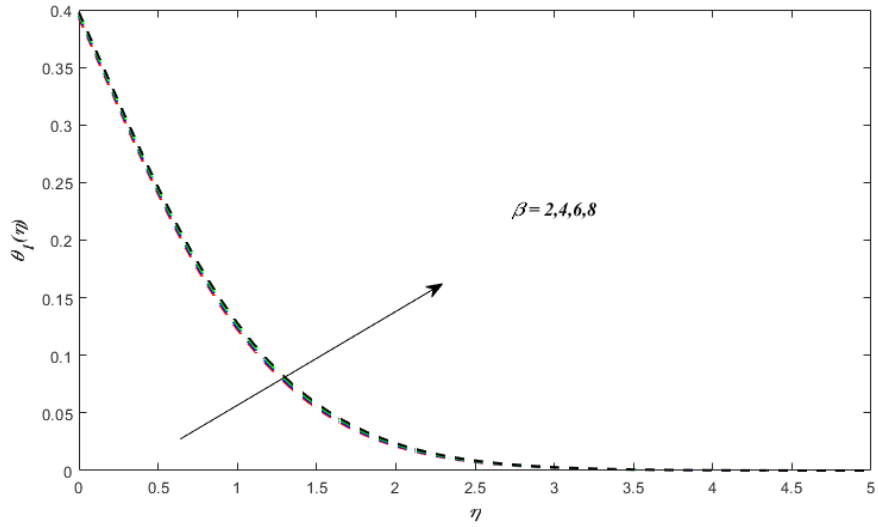

Fig. 4.5 Graph representing effect of θ_1 for several values of β

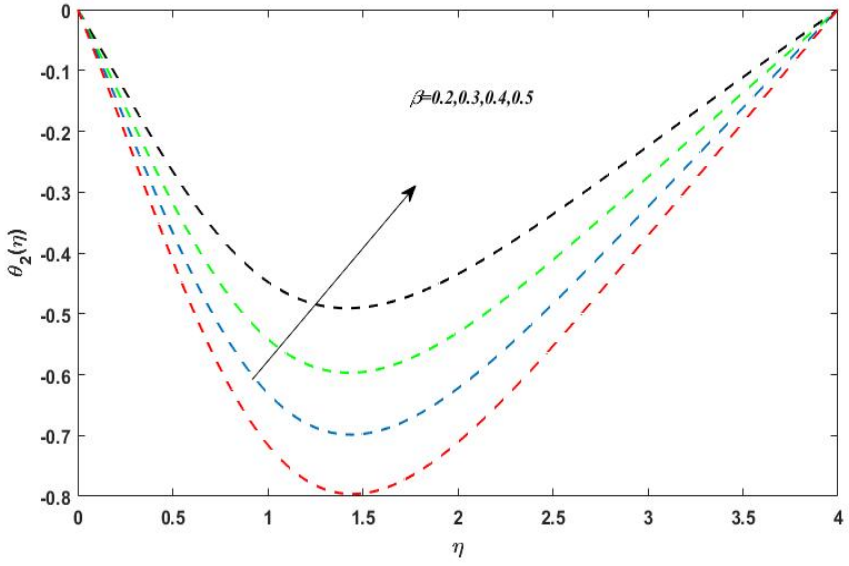

Fig. 4.6 Graph representing effect of θ_2 for several of β.

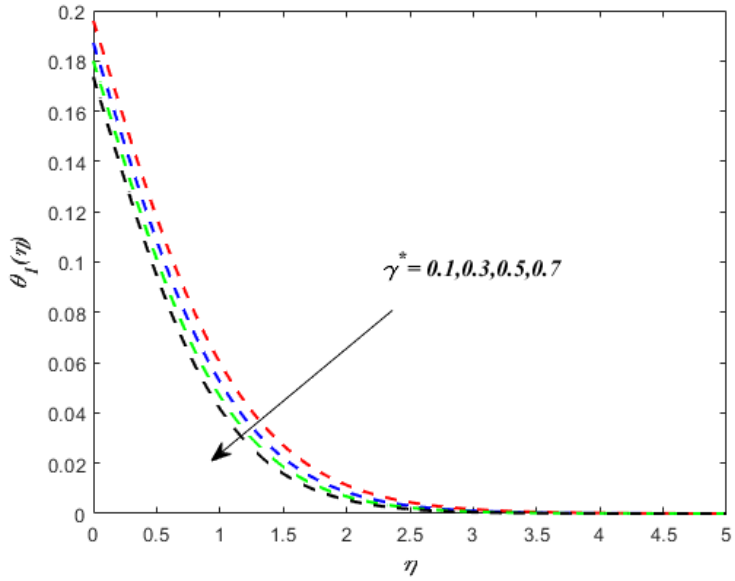

Fig. 4.7 Graph representing effect of θ_1 for several values of γ^*.

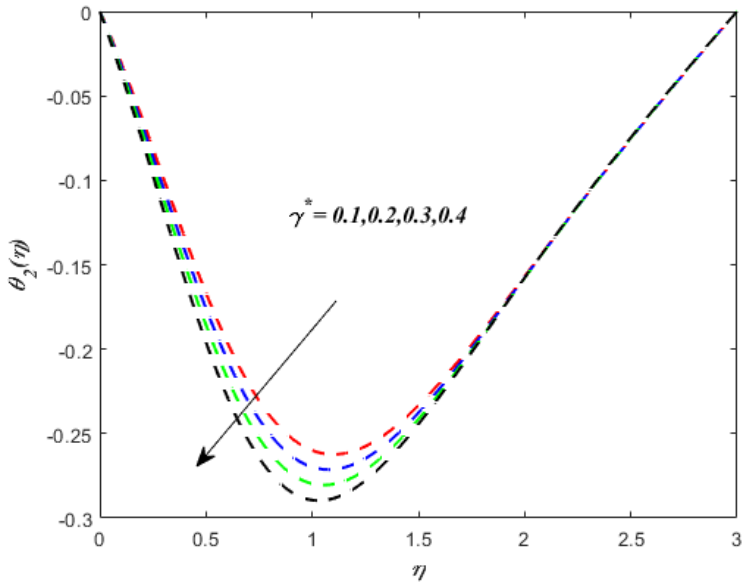

Fig. 4.8 Graph representing effect of θ_2 for several values of γ^*.

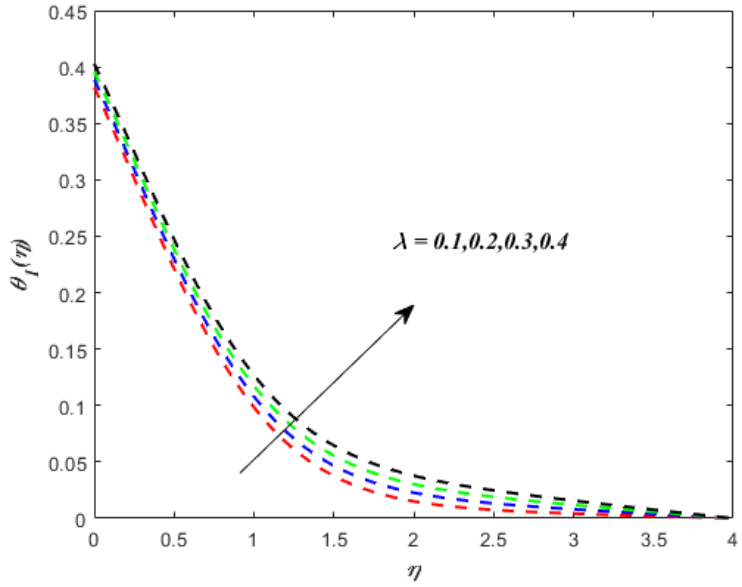

Fig. 4.9 Graph representing effect of θ_1 for several values of λ.

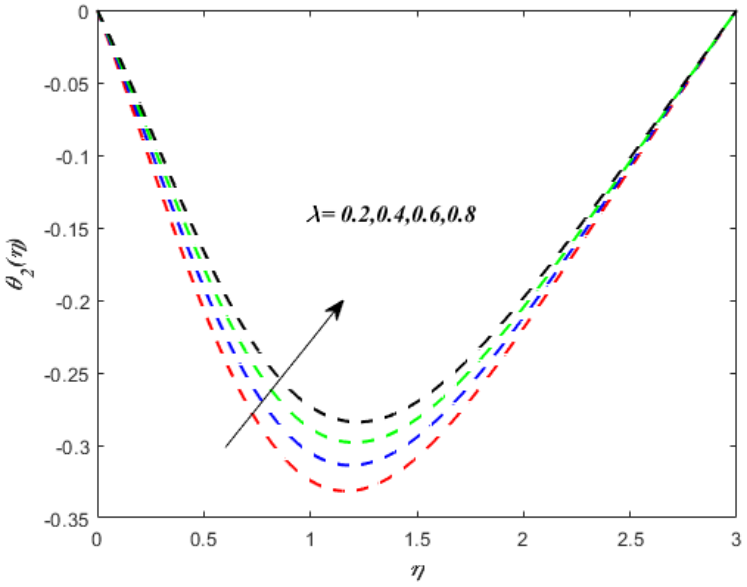

Fig. 4.10 Graph representing effect of θ_2 for several values of λ.

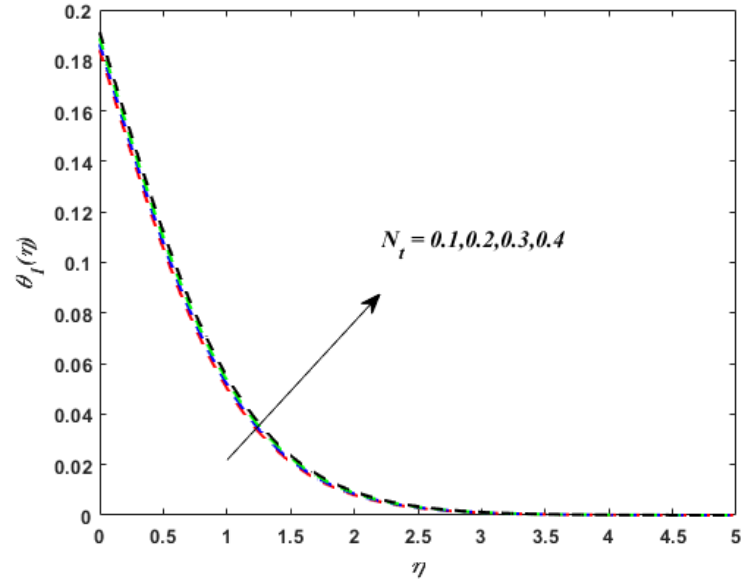

Fig. 4.11 Graph representing effect of θ_1 for several values of N_t.

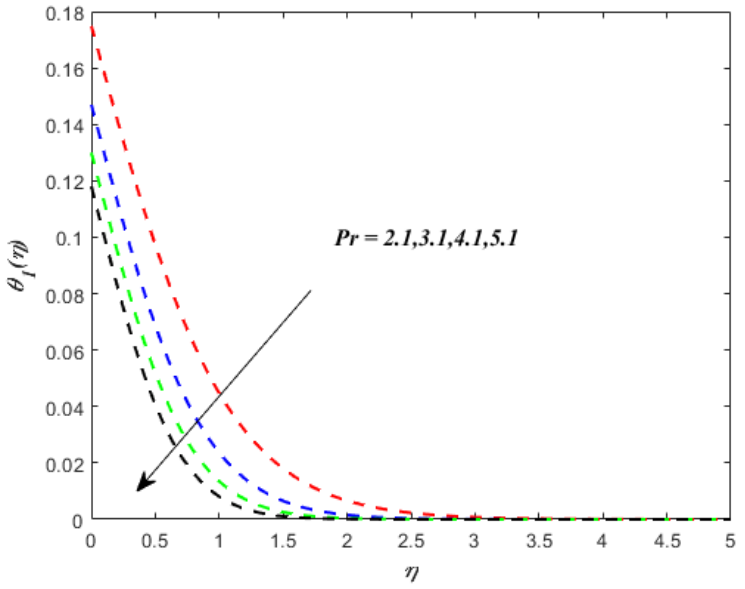

Fig. 4.12 Graph representing effect of θ_1 for several values of Pr .

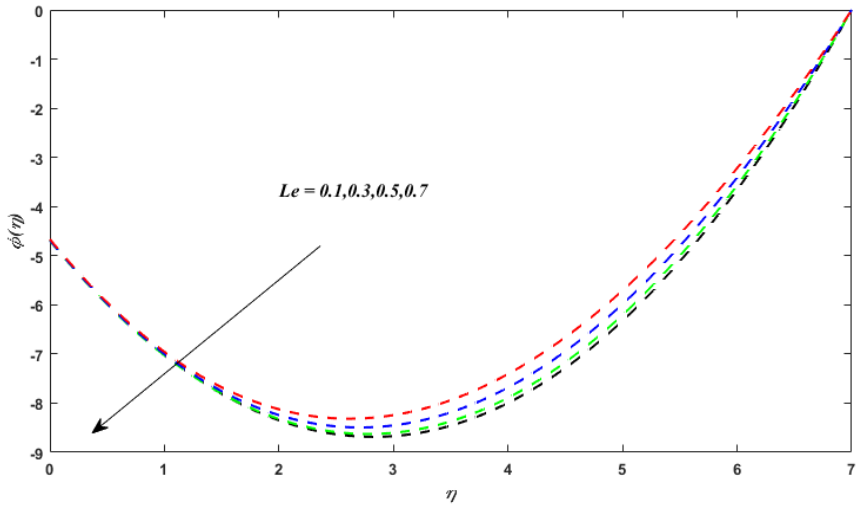

Fig. 4.13 Graph representing effect of ϕ for several values of Le.

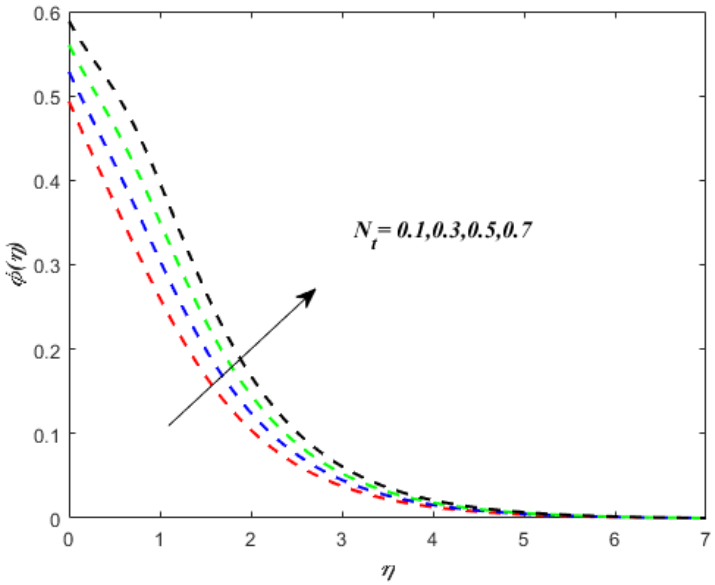

Fig. 4.14 Graph representing effect of ϕ for several values of N_t.

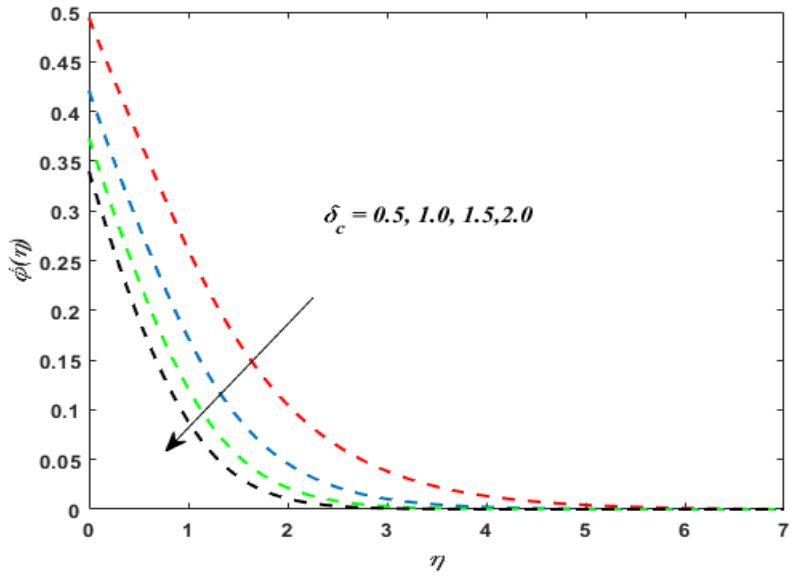

Fig. 4.15 Graph representing effect of ϕ for several values of δ_c.

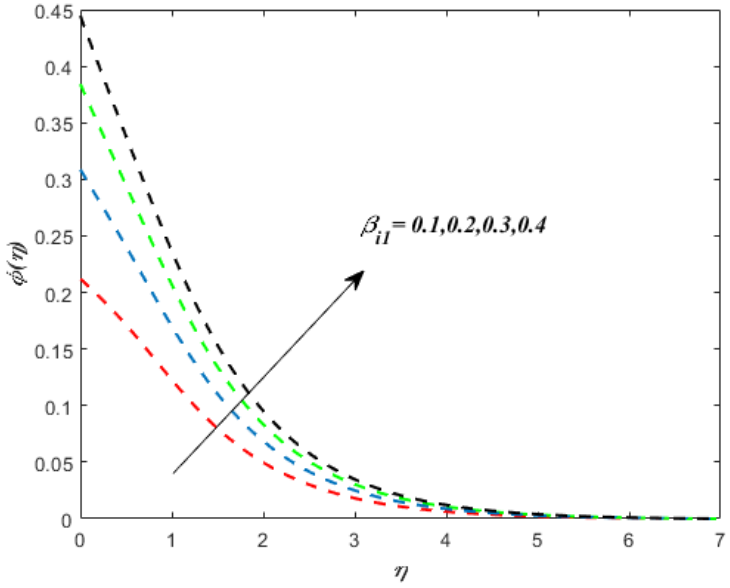

Fig. 4.16 Graph representing effect of ϕ for several values of β_{i1}.

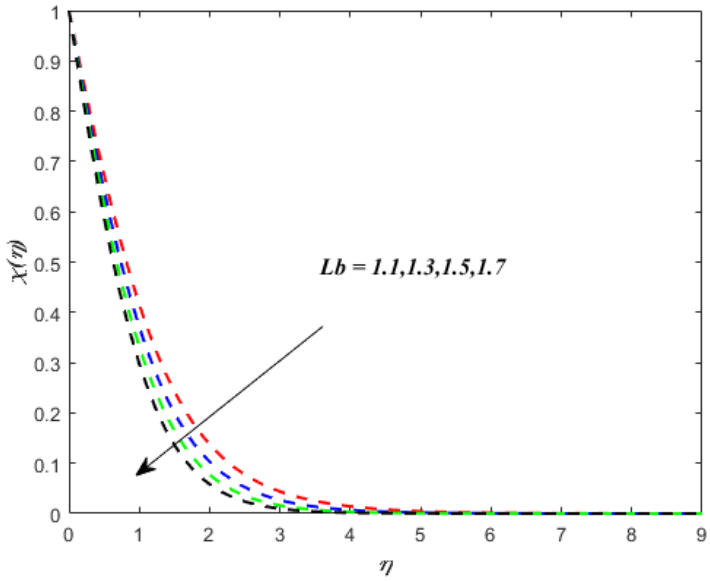

Fig. 4.17 Graph representing effect of χ for several values of Lb.

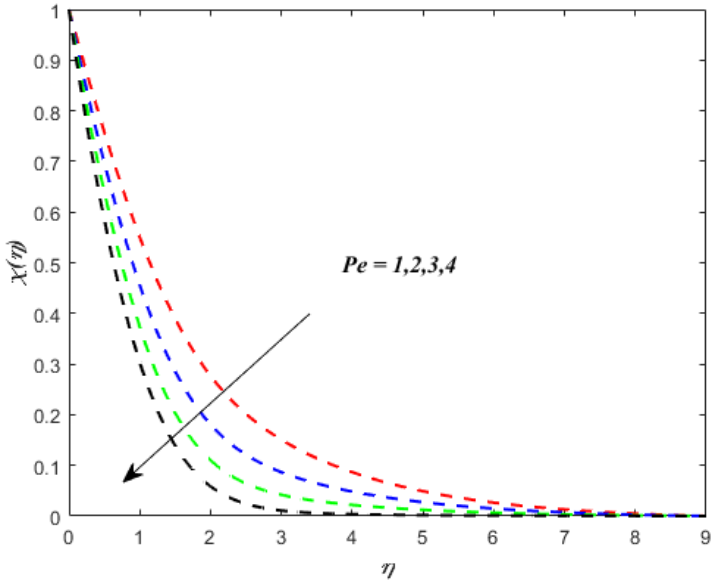

Fig. 4.18 Graph representing effect of χ for several values of Pe.

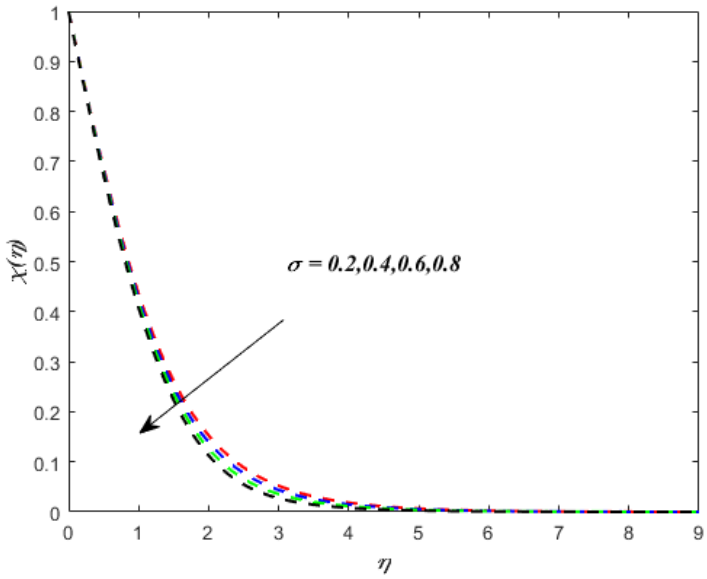

Fig. 4.19 Graph representing effect of χ for several values of σ.

Chapter 5

CONCLUSION AND FUTURE WORK

The first problem in this thesis is review work, and the second problem is extension work, both of which have been studied. The conclusion to both problem are as follows.

5.1 Review work

- In comparison to increased estimations of the ferromagnetic parameter, the temperature profiles, and velocity profiles show a reverse tendency.
- The Brownian motion parameter displays a falling trend in the concentration profile, while the thermophoretic parameter shows the opposite trend.
- The temperature ratio parameter reduces entropy generation, whereas the diffusion variable and Brinkman number increase entropy generation.
- The thermal of the fluid drops for large rising values of the melting heat parameter. The heated fluid actually transfers more heat to the surface when melting heat parameter values are high. In due course, the fluid temperature begins to decline.
- The enhanced heat-generating parameter results in the rise of fluid temperature.

5.2 Contribution of thesis

The following are the major findings of this study:

- The thermophoresis parameter N_t indicates the rising behaviour for both temperature and concentration profiles.
- The microorganisms in the density profile decrease as the Lewis number Lb, bio-convection Peclet number Pe, and microorganism concentration difference parameter increase σ.
- The expansion in Pr has adverse consequences for the temperature distribution.
- The Ferrohydrodynamic interaction parameter β has a positive impact on the temperature field, while having an adverse consequence on velocity dissemination.
- When the values of concentration relaxation parameter δ_c and Lewis number Le are increased, the boundary layer thickness and its related nanoparticle concentration are also decreased.
- The Viscous dissipation factor λ has a positive impact on the thermal profile.
- The increase in dimensionless thermal relaxation time γ^* corresponds to the thermal profile decline.
- As Biot number β_{i1} increase, the yield to the boundary layer thickness is increased together with the concentration field.

5.3 Future work

For future work, following may be considered:

- The Jeffrey fluid may be replaced with any other non-newtonian fluid.
- The boundary conditions may also be replaced with temperature and solutal stratifications.
- The magnetic dipole may be replaced with Hall and Ion slip effects.

Bibliography

[1] Ramzan, M., Bilal, M., Chung, J. D., Lu, D. C., & Farooq, U. Impact of generalized Fourier's and Fick's laws on MHD 3D second grade nanofluid flow with variable thermal conductivity and convective heat and mass conditions. Physics of Fluids, 29(9), pp. 093102, 2017.

[2] Das, S. K., Choi, S. U., Yu, W., & Pradeep, T. Nanofluids: science and technology. John Wiley & Sons, 2007.

[3] Safwa Khashi'ie, N., Md Arifin, N., Hafidzuddin, E. H., & Wahi, N. Dual stratified nanofluid flow past a permeable shrinking/stretching sheet using a non-Fourier energy model. Applied Sciences, 9(10), pp. 2124, 2019.

[4] Irfan, M., Khan, M., & Khan, W. A. Heat sink/source and chemical reaction in stagnation point flow of Maxwell nanofluid. Applied Physics A, 126(11), pp.1-8, 2020.

[5] Khan, M., Irfan, M., & Khan, W. A. Impact of nonlinear thermal radiation and gyrotactic microorganisms on the Magneto-Burgers nanofluid. International Journal of Mechanical Sciences, 130, pp. 375-382, 2017.

[6] Irfan, M., Khan, M., & Khan, W. A. Impact of non-uniform heat sink/source and convective condition in radiative heat transfer to Oldroyd-B nanofluid: a revised proposed relation. Physics Letters A, 383(4), pp. 376-382, 2019.

[7] Raju, C. S. K., Sandeep, N., & Gnaneswara Reddy, M. Effect of nonlinear thermal radiation on 3D Jeffrey fluid flow in the presence of homogeneous–heterogeneous reactions. In

International Journal of Engineering Research in Africa Trans Tech Publications Ltd, Vol. 21, pp. 52-68, 2016.

[8] T. Hayat, G. Bashir, M. Waqas and A. Alsaedi MHD flow of Jeffrey liquid due to a nonlinear radially stretched sheet in presence of Newtonian heating, Results in Physics 6, pp. 817-823, 2016.

[9] T. Hayat, M. Waqas, M. I. Khan and A. Alsaedi Impacts of constructive and destructive chemical reactions in magnetohydrodynamic (MHD) flow of Jeffrey liquid due to nonlinear radially stretched surface, Journal of Molecular Liquids 225 , pp. 302-310, 2017.

[10] M. A. Imran, F. Miraj, I. Khan and Tlili MHD fractional Jeffrey's fluid flow in the presence of thermo diffusion, thermal radiation effects with first order chemical reaction and uniform heat flux, Results in Physics 10, pp. 10-17, 2018.

[11] M. Waqas, S. A. Shehzad, T. Hayat, M. I. Khan and A. Alsaedi, Simulation of magneto hydro dynamics and radiative heat transport in convectively heated stratified flow of Jeffrey nanofluid, Journal of Physics and Chemistry of Solids 133, pp. 45-51.6, 2019.

[12] Zeeshan, A., & Majeed, A. Heat transfer analysis of Jeffery fluid flow over a stretching sheet with suction/injection and magnetic dipole effect. Alexandria engineering journal, 55(3), pp. 2171-2181, 2016.

[13] M. A. Imran, F. Miraj, I. Khan and Tlili MHD fractional Jeffrey's fluid flow in the presence of thermo diffusion, thermal radiation effects with first order chemical reaction and uniform heat flux, Results in Physics 10, pp. 10-17, 2018.

[14] Christov, C. I. On frame indifferent formulation of the Maxwell–Cattaneo model of finite-speed heat conduction. Mechanics Research Communications, 36(4), pp. 481-486, 2009.

[15] Khan, J. A., Mustafa, M., Hayat, T., Sheikholeslami, M., & Alsaedi, A. Three-dimensional flow of nanofluid induced by an exponentially stretching sheet: An application to solar energy. PloS one, 10(3), e0116603, 2015.

[16] Ramzan, M., Bilal, M., & Chung, J. D. Effects of MHD homogeneous-heterogeneous reactions on third grade fluid flow with Cattaneo-Christov heat flux. Journal of Molecular Liquids, 223, pp. 1284-1290, 2016.

[17] Rubab, K., & Mustafa, M. Cattaneo-Christov heat flux model for MHD three-dimensional flow of Maxwell fluid over a stretching sheet. PLoS One, 11(4), e0153481,2016.

[18] Tibullo, V., & Zampoli, V. A uniqueness result for the Cattaneo–Christov heat conduction model applied to incompressible fluids. Mechanics Research Communications, 38(1), pp. 77-79, 2011.

[19] Zeeshan, A., Majeed, A., & Ellahi, R. Effect of magnetic dipole on viscous ferro-fluid past a stretching surface with thermal radiation. Journal of Molecular liquids, 215, pp. 549-554, 2016.

[20] Zeeshan, A., & Majeed, A. (2016). Heat transfer analysis of Jeffery fluid flow over a stretching sheet with suction/injection and magnetic dipole effect. Alexandria engineering journal, 55(3), pp. 2171-2181, 2016.

[21] Ali, L., Liu, X., Ali, B., Mujeed, S., Abdal, S., & Khan, S. A. Analysis of magnetic properties of nano-particles due to a magnetic dipole in micropolar fluid flow over a stretching sheet. Coatings, 10(2), pp.170, 2020.

[22] Kumar, R. N., Jyothi, A. M., Alhumade, H., Gowda, R. P., Alam, M. M., Ahmad, I., ... & Prasannakumara, B. C. Impact of magnetic dipole on thermophoretic particle deposition in the flow of Maxwell fluid over a stretch, 2021.

[23] Naveen Kumar, R., Suresha, S., Gowda, R. J., Megalamani, S. B., & Prasannakumara, B. C. Exploring the impact of magnetic dipole on the radiative nanofluid flow over a stretching sheet by means of KKL model. Pramana, 95(4), pp. 1-9, 2021.

[24] Khan, N. S., Usman, A. H., Sohail, A., Hussanan, A., Shah, Q., Ullah, N., ... & Humphries, U. W. A framework for the magnetic dipole effect on the thixotropic nanofluid flow past a continuous curved stretched surface. Crystals, 11(6), 645. ing sheet. Journal of Molecular Liquids, 334, pp. 116494, 2021.

[25] Raju, C. S. K., Hoque, M. M., & Sivasankar, T. Radiative flow of Casson fluid over a moving wedge filled with gyrotactic microorganisms. Advanced Powder Technology, 28(2), pp. 575-583, 2017.

[26] Chamkha, A.J.; Rashad, A.M.; Kameswaran, P.K.; Abdou, M.M. Radiation effects on natural bioconvection flow of a nanofluid containing gyrotactic microorganisms past a vertical plate with streamwise temperature variation. J. Nanofluids 6, pp. 587–595, 2017.

[27] Akbar, N. S., & Khan, Z. H. Magnetic field analysis in a suspension of gyrotactic microorganisms and nanoparticles over a stretching surface. Journal of Magnetism and Magnetic materials, 410, pp. 72-80, 2016.

[28] Waqas, H., Khan, S. U., Hassan, M., Bhatti, M. M., & Imran, M. Analysis on the bioconvection flow of modified second-grade nanofluid containing gyrotactic microorganisms and nanoparticles. Journal of Molecular Liquids, 291, pp. 111231, 2019.

[29] Khan, N.S. Bioconvection in second grade nano fluid flow containing nanoparticles and gyrotactic microorganisms. Braz. J. Phys. 48, pp. 227–241, 2018.

[30] Ferdows, M.; Zaimi, K.; Rashad, A.M.; Nabwey, H.A. MHD bioconvection fluid flow and heat transfer of nanofluid through an exponentially stretchable sheet. Symmetry 12, pp. 692, 2020.

[31] Khan, S.U.; Al-Khaled, K.; Bhatti, M.M. Bioconvection analysis for fluid flow of Oldroyd-B nanofluid configured by a convectively heated surface with partial slip effects. Surf. Interfaces 23, pp. 100982, 2021.

[32] Majeed, A.; Zeeshan, A.; Amin, N.; Ijaz, N.; Saeed, T. Thermal analysis of radiative bioconvection magneto hydro dynamic fluid flow comprising gyrotactic microorganism with activation energy. J. Therm. Anal. Calorim. 143, pp. 2545–2556, 2021.

[33] Chen, C. H. Laminar mixed convection adjacent to vertical, continuously stretching sheets. Heat and Mass transfer, 33(5), pp. 471-476, 1998.

[34] Chen, X., Ye, Y., Zhang, X., & Zheng, L. Lie-group similarity solution and analysis for fractional viscoelastic MHD fluid over a stretching sheet. Computers & Mathematics with Applications, 75(8), pp. 3002-3011, 2018.

[35] Ramzan, M., Howari, F., Chung, J. D., Kadry, S., & Chu, Y. M. Irreversibility minimization analysis of ferromagnetic Oldroyd-B nanofluid flow under the influence of a magnetic dipole. Scientific Reports, 11(1), pp.1-19, 2021.

Iqra thesis

ORIGINALITY REPORT

12%	5%	8%	4%
SIMILARITY INDEX	INTERNET SOURCES	PUBLICATIONS	STUDENT PAPERS

PRIMARY SOURCES

1	Submitted to Higher Education Commission Pakistan Student Paper	3%
2	Muhammad Ramzan, Fares Howari, Jae Dong Chung, Seifedine Kadry, Yu-Ming Chu. "Irreversibility minimization analysis of ferromagnetic Oldroyd-B nanofluid flow under the influence of a magnetic dipole", Scientific Reports, 2021 Publication	2%
3	www.nature.com Internet Source	1%
4	www.ncbi.nlm.nih.gov Internet Source	1%
5	Hao Cui, Corby G. Anderson. "Alternative flowsheet for rare earth beneficiation of Bear Lodge ore", Minerals Engineering, 2017 Publication	<1%
6	Muhammad Naveed Khan, Haneen Hamam, Fehmi Gamaoun, Awatif Alhowaity, Mansour F. Yassen, Hassan Ali Ghazwani. "Heat and	<1%

Ramz 30/09/2022